NJC

PAPER

View Article Online
View Journal

Cite this: DOI: 10.1039/c4nj02011a

Optically active, three-ring calamitic liquid crystals: the occurrence of frustrated, helical and polar fluid mesophases

B. N. Veerabhadraswamy, D. S. Shankar Rao, S. Krishna Prasad and C. V. Yelamaggad*

Herein, we report on the synthesis, characterization, liquid crystalline behavior and chirooptical properties of five (*R*)-4-{[(4-(octan-2-yloxy)phenyl)imino]methyl}phenyl 4-(*n*-alkoxy)benzoates and their enantiomers, namely, (*S*)-4-{[(4-(octan-2-yloxy)phenyl)imino]methyl}phenyl 4-(*n*-alkoxy)benzoates. These three-ring rod-like mesogens were prepared by acid catalyzed condensation of (*R*)-/(*S*)-4-(octan-2-yloxy)anilines with 4-formylphenyl 4-(*n*-alkoxy)benzoates. Thus, each pair of enantiomers comprises (*R*)-2-octyloxy and (*S*)-2-octyloxy chiral tails. In order to understand the structure–property correlations, the length of the paraffinic chain incorporated at the other end has been varied from *n*-octyloxy to *n*-dodecyloxy. A detailed study carried out by means of several complimentary techniques reveals the stabilization of liquid crystal phases that hold great promise in applied sciences especially in various device applications. In particular, the occurrence of mesophases such as the blue phase-I/II (BPI or BPII) and chiral nematic (N*) and chiral smectic C (SmC*) phases has been evidenced unequivocally with the help of polarizing microscopy, differential scanning calorimetry, X-ray diffraction and electrical switching. Besides, the occurrence of an unknown, metastable smectic (SmX) phase below the SmC* phase has been noted. This study shows that the length of the terminal tail seems to determine the thermal range of the SmC* phase. The enantiotropic SmC* phase exhibiting ferroelectric switching behavior occurs over 60 °C thermal range; notably, the spontaneous polarization (P_s) value crosses over 100 nC cm^{-2}. The photophysical properties and chirooptical behavior of the mesogens have been studied with the aid of UV-vis absorption and circular dichroism (CD) spectroscopic methods, respectively; the latter technique has been especially used to ascertain the twist sense of the N* and SmC* phases formed by a pair of enantiomers. The reversal of the helix-sense (from right to left and *vice versa*) during the N*–SmC* phase transition has been observed for the first time.

Received (in Porto Alegre, Brazil) 11th November 2014,
Accepted 6th January 2015

DOI: 10.1039/c4nj02011a

www.rsc.org/njc

1. Introduction

Over the past several decades, thermotropic liquid crystalline organic or metallo-organic compounds (mesogens) composed of shape-anisotropic molecules exhibiting liquid crystal (LC) phases (mesomorphism), upon heating, have attracted much attention from both researchers and technologists.[1] This is mainly because the LC phases, being liquid in mobility and crystalline in their anisotropic physical properties, are highly beneficial and rewarding in the context of both basic science[1] and applied research.[1,2] It is especially noteworthy in the case of chiral LC phases that are formed by pure mesogens possessing asymmetric carbon atom(s) rendering molecular chirality (symmetry concept) or by the influence of guest chiral dopants (which may or may not be LC) on the host achiral LC phases. These bulk aggregates, besides combining the order and mobility on a molecular (nano scale) level, stabilize frustrated phases and helical superstructures besides some chiral layered structures.[3,4] Frustrated LC phases such as twist grain boundary (TGB) phases and blue phases (BPs) have evoked considerable curiosity on account of their structural complexity stemming from the molecular self-assembly into two incompatible (layered and helicoidal) structures, which is eventually achieved by the formation of lattice defects. Whereas, the defect free helical superstructures such as chiral nematic (N*) or chiral smectic C (SmC*) with a spectrum of unique properties have been used as sources (media) for device applications in various sectors.[1,3,4] The SmC* phase, for instance, exhibiting ferroelectric switching behaviour,[3,4] wherein the spontaneous polarisation (P_s) resulting from the specific structure formed by the self-assembly of chiral mesogens

Centre for Nano and Soft Matter Sciences (Formerly Centre for Soft Matter Research), Prof. U. R. Rao Road, Post Box No. 1329, Jalahalli, Bangalore 560 013, India. E-mail: yelamaggad@cnsms.com; Fax: +91-80-28382044; Tel: +91-80-23084-233

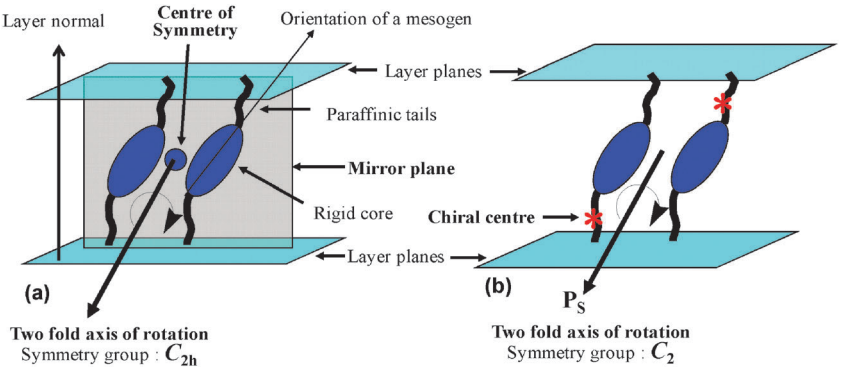

Fig. 1 Symmetry in the smectic C (a) and chiral smectic C (b) phases.

can be reoriented upon application of an electric field, has been used for fabricating display devices as it offers added benefits when compared to classical LC displays (LCDs) derived from the nematic (N) phase. For example, high image quality, fast response time (in micro-seconds), optical bistability, high resolution and wide-viewing angles *etc.* are some of the well-known advantages of ferroelectric LCDs.[4]

The smectic C (SmC) phase differs from the SmC* phase in that the director of each layer is inclined at an angle to the layer normal and this angle being the same for all layers. The tilt angle in this phase alters with temperature and it generally increases with decreasing temperature. As shown in Fig. 1a, it is characterized by a centre of symmetry, a two-fold axis of rotation and a mirror plane normal to the two-fold axis; the symmetry elements correspond to the point group C_{2h}.[1] When the SmC phase is generated by chiral mesogens or mixed with chiral dopants, it becomes optically active where a macroscopic helical arrangement of the constituent mesogens occurs spontaneously.[3–5] In fact, the helix occurs as a result of a gradual change in the molecular tilt direction (n) from layer to layer, about an axis perpendicular to the layer planes. Owing to the presence of chiral molecules, the local symmetry reduces to a two-fold axis of rotation, which creates inequivalence in the dipole moment along the C_2 axis normal to the tilt direction (Fig. 1b), giving rise to spontaneous polarization (P_s) in each layer. However, on a macroscopic level there is no net polarization as the helix averages out the P_s to zero. Therefore, the bulk SmC* phase is appropriately termed 'helielectric' instead of ferroelectric. Nonetheless, to realize a macroscopic polarization the helix should be unwound by an external force such as an electric field or shear or by surface interaction and thereby the bulk SmC* phase becomes ferroelectric where the helical structure is deformed. As mentioned earlier, this behavior of the SmC* phase has been well exploited in developing high-resolution micro-displays that are successfully used in a range of devices *viz.*, color viewfinders in digital cameras, camcorders, pico-projectors, medical imaging *etc.*[4,5]

However, the usage of ferroelectric technology in the present and future advanced devices, needless to say, depends to a large degree on the availability of suitable materials capable of showing a wide thermal span of the requisite mesophase, preferably from higher temperature to sub-ambient temperature,[6] possessing a low viscosity and a high magnitude of P_s.[4,5,7] Despite the fact that a range of ferroelectric LCs (FLCs) have been accomplished through rational design and synthesis since 1975,[4,5,7] it has been an extremely difficult assignment to find the materials exhibiting the optimum physical properties in pure, single component systems.[7] However, multi-component systems made by doping an achiral host mixture with highly polar chiral compounds are proven to be helpful in meeting the material properties required for device fabrication; thus, this means of obtaining suitable FLCs is still followed to a large extent.[8] Yet, this approach also suffers from technical issues as there are only a limited number of host SmC LCs suitable to utilize[4a] although a large number of efforts have been explored in this regard;[9] besides, finding a chiral dopant possessing a high P_s, and a long chiral nematic pitch appears to be bothersome. Moreover, the compatibility among host LC and the chiral dopant is a major concern; in other words, the multi-component systems should be free from phase separation problem. Besides, figuring out exact molar concentrations of the guest material and host LC(s) to meet the desired properties is highly time-consuming and quite tricky. Therefore, there have been continued, extensive efforts into the design and synthesis of ferroelectric LCs basically to understand the structure–property correlations, which may eventually facilitate to arrive at a well-defined, one-component chiral LC having all of the desired characteristics; such a chiral compound has an added advantage as it can also be used as a dopant for the host SmC phase. Thus, in continuation of our work on chiral LCs,[10–16] we became interested in realizing new FLCs.

Accordingly, we designed and prepared rather simple (overlooked) chiral calamitics comprising three-rings covalently tethered to one another linearly through two polar linking groups. The present molecular design originated from the guide lines available in the literature to generate mesogens competent of stabilizing the SmC*/SmC phase.[3–5,7,17,18] The accumulated knowledge concerning structure–property correlations suggest that a rigid, polarisable rod-like (long) core, having two or three-rings substituted with relatively long paraffinic chains at both the ends, favours the molecular self-assembly into the smectic phases. If the central linking groups possess a dipole moment normal to the long axis of the molecules, they provide lateral polarity to induce molecular self-assembly into layers and also assist

molecular tilting with respect to layer normal; thereby the SmC phase can be stabilized. The ester (–COO–) and imine (–CH=N–) groups are well-known examples of linking units that induce lateral polarity effectively.[4a,7,18e] Indeed, in order to reduce the local symmetry to a two-fold axis of rotation to account for polarization in each layer, the chirality in molecules, which is necessary to be introduced, can be achieved, needless to say, by replacing one (or both) of the achiral tails with the chiral chain. Furthermore, there is an experiential notion that the magnitude of polarization can be improved significantly if the stereocentre is placed nearer to the rigid-core;[17] the hindered rotation of a chiral moiety with respect to the core appears to yield a high P_s value.[17c] It is also perceptible from the literature that three-ring systems favour the SmC*/SmC structures.[18] Thus, these aspects were considered while designing the present molecules to maximize the likelihood of required mesophase stabilization. Here, we present the synthesis and mesomorphic properties of five pairs of enantiomers in which three-benzene rings are bound linearly to each other through ester and imine linkages. The molecular structures of mesogens along with the abbreviations used are shown in Scheme 1; obviously, each pair of enantiomers comprises (*R*)-2-octyloxy and (*S*)-2-octyloxy terminal tails; the length of the achiral, paraffinic chain incorporated at the other end has been varied from *n*-octyloxy to *n*-dodecyloxy with the aim of studying the correlations between molecular structure and thermal property, especially in terms of stabilizing the SmC* phase.

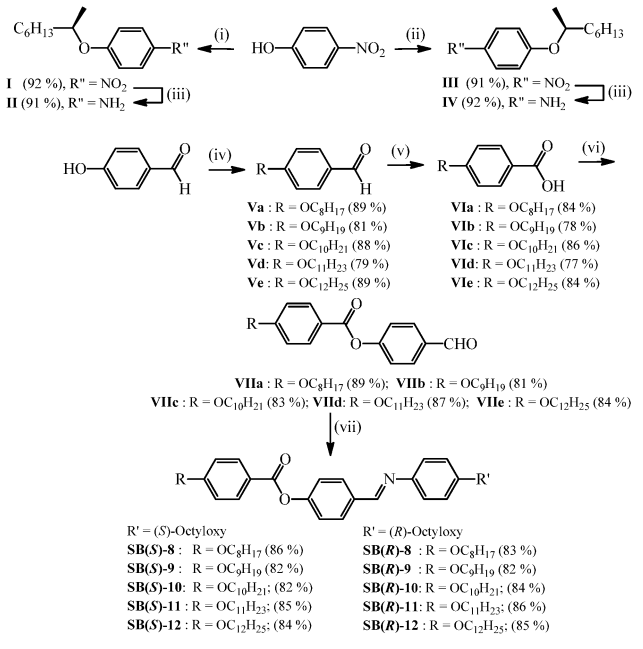

Scheme 1 Synthesis of chiral, three-ring rod-like LCs. *Reagents & conditions*: (i) (*S*)-(+)-2-octanol, Ph_3P, DIAD, THF, rt, 18 h; (ii) (*R*)-(−)-2-octanol, Ph_3P, DIAD, THF, rt, 18 h; (iii) H_2, (1 atm, ballon), 10% Pd–C, THF, rt, 4 h; (iv) *n*-bromo-alkane, anhydrous K_2CO_3, DMF, 80 °C, 12 h. (v) Jones reagent, acetone, rt, 1 h; (vi) 4-hydroxybenzaldehyde, DCC, DMAP, THF, rt, 4 h. (vii) **II** & **IV**, EtOH, AcOH, reflux, 5 h.

2. Results and discussion

2.1. Synthesis and molecular structural characterization

The target chiral rod-like Schiff bases were prepared according to Scheme 1. As can be seen, their synthesis required the preparation of key precursors (*R*) and (*S*)-4-(octan-2-yloxy)anilines (**II** and **IV**) and 4-formylphenyl 4-(*n*-alkyloxy)benzoates (**VIIa–e**). 4-Nitrophenol was *O*-alkylated with the chiral alcohols, (*S*)- and (*R*)-2-octanol, following the Mitsunobu reaction[19] to obtain (*R*)- and (*S*)-4-(octan-2-yloxy)-nitrobenzenes (**I** and **III**),[20] which were subjected to catalytic hydrogenation under the reaction conditions – H_2 (1 atm, balloon), Pd/C (10%), THF, to get the corresponding anilines **II** and **IV** in excellent yields.[20] Two-ring aldehydes **VIIa–e** were synthesized starting from commercially available 4-hydroxybenzaldehyde; it was *O*-alkylated with appropriate *n*-bromoalkane following the Williamson ether synthesis protocol to get 4-(*n*-alkoxy)benzaldehydes (**Va–e**)[14–16] which were oxidized with a Jones reagent to obtain corresponding 4-(*n*-alkoxy)benzoic acids (**VIa–e**);[21] these acids were esterified with 4-hydroxybenzaldehyde in the presence of *N*,*N*′-dicyclohexylcarbodiimide (DCC) and 4-dimethylaminopyridine (DMAP)[22] leading to key aldehydes **VIIa–e**.[23] The proposed mesogens, the three-ring Schiff bases (imines), were obtained in excellent (82–86%) yield when anilines **II** & **IV** and aldehydes **VIIa–e** were made to react with each other in refluxing ethanol in the presence of a catalytic amount (few drops) of acetic acid. The final compounds were characterized systematically by IR, UV-visible, ^{1}H and ^{13}C NMR spectroscopy and CHN analyses. While the intermediates have been characterized with the help of IR and ^{1}H NMR spectroscopy and elemental microanalyses only; the data of the known intermediates were found to be consistent with that of reported ones.

2.2. Evaluation of phase transitional behavior

The mesomorphism of the newly synthesized chiral mesogens was examined with the aid of optical microscopic, calorimetric, X-ray diffraction (XRD) and electro-optical studies. Table 1 presents the phase sequence, transition temperatures and enthalpies of the transitions; here, the phase transition temperatures deduced from calorimetric measurements of the first heating–cooling cycles at a rate of 5 °C min^{-1} are given. When the peaks are not seen in DSC traces, the phase transition temperatures noted during the POM study are taken. From the accumulated data it is apparent that all the mesogens synthesized exhibit an identical phase transitional behaviour; during the heating cycle they show three thermodynamically stable mesophases which have been identified as BP-I/II, N* and SmC* phases; an unusual, monotropic mesophase, hereafter referred to as the SmX phase, is seen additionally, while cooling the samples from their isotropic phase. Most importantly, the SmC* phase, existing over 60 °C thermal span, shows ferroelectric switching property with the P_s value of about 100 nC cm^{-2}. It seems, therefore, that the present simple molecular architecture, which has been overlooked hitherto, supports the stabilization of the SmC* phase convincingly. The details of these experimental investigations with analysis of the results are discussed below.

2.2.1. Microscopic and calorimetric studies. Liquid crystallinity of all the five pairs of enantiomers was first ascertained based on the textural observation where the characteristic optical birefringence

Table 1 Phase transition temperatures (°C)[a] and associated enthalpies (kJ mol^{-1}) of transitions noted for three-ring rod-like **SB(*S*)-*n*** and **SB(*R*)-*n*** series of compounds. • = enantiotropic phase; (•) = monotropic LC phase. Cr: crystal; SmX: unknown smectic phase; SmC*: chiral smectic C phase; N*: chiral nematic phase; BP = blue phase-I or blue phase-II

LCs	Cr	Heating Cooling	SmX	Heating Cooling	SmC*	Heating Cooling	N*	Heating Cooling	BP	Heating Cooling	I
SB(*S*)-8	•	84.5 [41.9] 53.6 [26.9]	(•)	— 59.5 [4.2]	•	122.2 [0.4] 121.3 [0.4]	•	147.9 [0.8] 147.1 [0.8][b]	•	— 147.6	•
SB(*R*)-8	•	87.2 [41.3] 54.9 [23.4]	(•)	— 59.4 [3.9]	•	122.3 [0.4] 121.4 [0.4]	•	148.0 [0.7] 147.0 [0.8][b]	•	— 147.3	•
SB(*S*)-9	•	86.1 [34.6] 54.9 [21.8]	(•)	— 58.6 [4]	•	124.8 [0.8] 123.7 [0.8]	•	144.2 [0.8] 143.2 [0.8][b]	•	— 143.7	•
SB(*R*)-9	•	85.9 [31.9] 55.8 [11.1]	(•)	— 58.7 [3.8]	•	124.6 [0.8] 123.8 [0.7]	•	143.9 [0.8] 143.1 [0.8][b]	•	— 143.4	•
SB(*S*)-10	•	78.0 [36.2] 31.7 [19.9]	(•)	— 64.8 [5.1]	•	127.9 [0.9] 126.9 [1.0]	•	142.8 [1.0] 141.8 [1.0][b]	•	— 142.2	•
SB(*R*)-10	•	74.6 [3.2][c] 31.0 [22.1]	(•)	— 64.9 [5.8]	•	127.6 [1.0] 126.8 [0.9]	•	142.5 [1.1] 141.7 [1.0][b]	•	— 142.0	•
SB(*S*)-11	•	66.8 [28.4] 24.7 [15.6]	(•)	— 60.2 [4.4]	•	128.1 [1.2] 127.1 [1.2]	•	139.0 [1.1] 138.0 [1.1]	•	— 138.3	•
SB(*R*)-11	•	68.5 [33.9] 25.3 [15.4]	(•)	— 60.0 [4.3]	•	128.4 [1.2] 127.3 [1.2]	•	139.3 [1.1] 138.2 [1.1][b]	•	— 138.6	•
SB(*S*)-12	•	63.8 [43.3] —	(•)	— 62.6 [4.9][d]	•	130.0 [1.4] 128.9 [1.4]	•	138.2 [1.3] 137.1 [1.3][b]	•	— 137.6	•
SB(*R*)-12	•	63.7 [37.4] —	(•)	— 62.9 [4.2][d]	•	130.1 [1.2] 129.1 [1.2]	•	138.3 [1.2] 137.4 [1.3][b]	•	— 137.8	•

[a] Transition temperatures determined by both a polarizing optical microscope (POM) and peak values of the DSC traces during the first heating–cooling cycles at 5 °C min^{-1} rate. [b] The I–BP and BP–N* phase transitions were seen under POM, but they were too weak to be detected by DSC; thus, the ΔH value represents the combined enthalpy for the I–BP and BP–N* transitions. [c] An additional Cr–Cr transition has been seen at 71.9 °C [47 kJ mol^{-1}]. [d] The SmX phase freezes into a glassy state near room temperature (~30 °C) that remains unaltered till −50 °C (limitation of the instrument).

coupled with spontaneous fluidity could be seen under POM;[24] for this purpose, the sample, under investigation, held between a clean untreated glass slide and a cover slip was used. For confirmation of the mesophase-type assignment, both homogeneously and homeotropically aligned samples were examined thoroughly. The microphotographs of the optical textures seen for the compounds under different experimental conditions are presented in Fig. 2, as representative cases. Likewise, the DSC thermograms recorded during first heating–cooling cycles of all the five pairs of enantiomers are shown in Fig. 3a. The peak temperatures of the phase transitions noted from the DSC traces of the heating–cooling cycles were found to be in complete agreement with those of the optical experiments. In fact, all the ten mesogens, although comprising imine linkage, were found to be thermally stable exhibiting virtually identical phase sequences with unaffected transition temperatures for any number of heating–cooling runs of both optical and calorimetric studies. Fig. 3b, for example, depicts the DSC traces obtained for the three consecutive heating–cooling cycles of an enantiomer where the aforesaid features can be visualized corroborating our remarks indubitably.

The optical textural patterns showed typical defects associated with LC phases such as BPI/II, N* and SmC* phases; the SmX also exhibited textures that were not enough to assign the structure. These samples, sandwiched between clean glass slides and cooled slowly from the isotropic phase, exhibit a LC phase with a striking textural pattern emanating from the black background of the isotropic phase that quickly fills the field of view (Fig. 2a) but exists for a very short thermal range. This texture, showing a brightly coloured pattern of individual, micron sized platelets, is typical of the BP-I/II phase;[3b,24] in fact, the bright colour indicates selective reflection due to the periodic structure. Upon cooling this phase, a transition to another mesophase occurs exhibiting an atypical textural pattern (Fig. 2b) which upon gentle shearing transformed into an oily streak pattern occurring over a planar texture (Fig. 2c) implying the presence of the N* phase;[24] in this planar texture, the helical axis is perpendicular to the glass plates, *i.e.*, along the viewing direction. It may be noted here that the BP–N* transition found to be too weak to be detected by DSC and therefore the enthalpy (ΔH) value, ranging between 0.8 to 1.3 kJ mol^{-1} (see Table 1), represents the combined ΔH for the I–BP and BP–N* transitions.

Upon further cooling from the unsheared N* phase, a mesophase appears displaying a texture comprising two different patterns originating from the planar and homeotropic orientations of molecules. It is apparent from the Fig. 2d that the planar region shows the concentric circular rings as well as broken focal-conics superimposed by the equidistant (dechiralization) lines. On the other hand, the homeotropic domains display a dull-grayish pattern; notably, at some edges of the cell a grayish schlieren-like texture was also seen (Fig. 2e). These optical textures observed are indeed the characteristics of the SmC* phase.[24] As can be seen in Table 1, the enthalpy of the N*–SmC* transition was found to be in the range of 0.4 to 1.4 kJ mol^{-1}. Upon further cooling, a sharp transition from the SmC* phase to the SmX phase occurs where the pseudo-isotropic pattern and distorted circular domains as well as the broken focal-conic fan texture (Fig. 2f) were seen due to the homogeneous and homeotropic orientations of the constituent mesogens, respectively. The presence of focal-conic domains suggests a layered arrangement, while the homeotropic

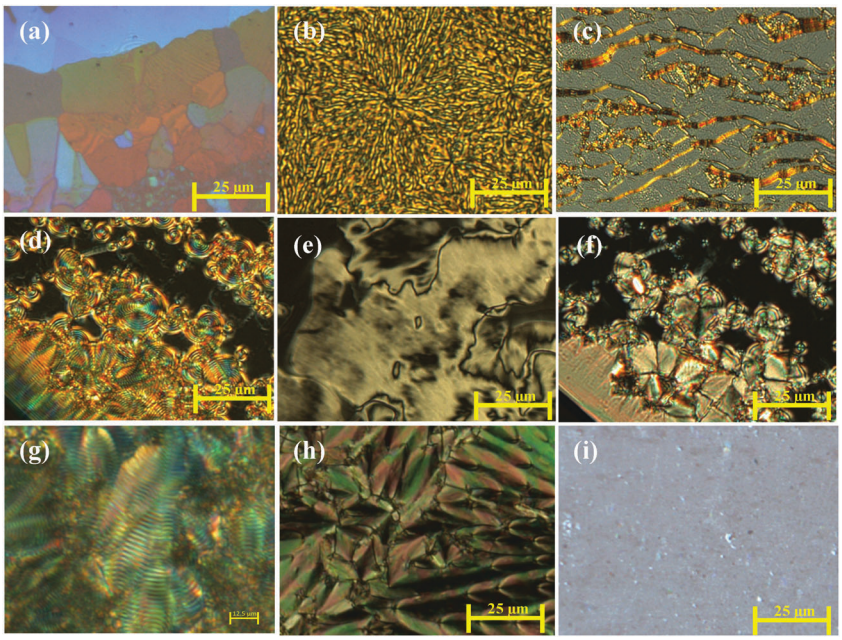

Fig. 2 Microphotographs of the optical textural patterns of the mesophases of **SB(*R*)-10** held between two untreated slides (a–f) and treated glass substrates (g–i): (a) the platelet texture of the BP-I/II occurring just below the isotropic phase (141.8 °C); (b) the vague texture obtained for the N* phase at 135 °C; (c) the typical oily streak texture of the N* phase formed at 130 °C when the pattern-(b) was sheared gently; (d) planarly, and homeotropically aligned SmC* phase showing the banded concentric circles as well as the banded broken focal-conic texture, and the intense dark-greyish pattern (115 °C), respectively; (e) the schlieren-like pattern found at the edge of the slide for the SmC* phase (115 °C); (f) the distorted circular domains as well as the broken focal-conic fan pattern and the pseudo-isotropic texture, respectively, observed for the homogeneously and homeotropically oriented SmX phase at 58 °C; (g) the occurrence of a classical fan-shaped texture, featuring equidistant lines on top of it, when the SmC* phase was subjected to planar boundary conditions; (h) the textural pattern seen at 58 °C for the planarly aligned SmX phase where focal-conics, fan-shaped pattern and polygonal domains can be seen; (i) the cloudy texture seen for the homeotropically oriented SmC* phase at 121 °C.

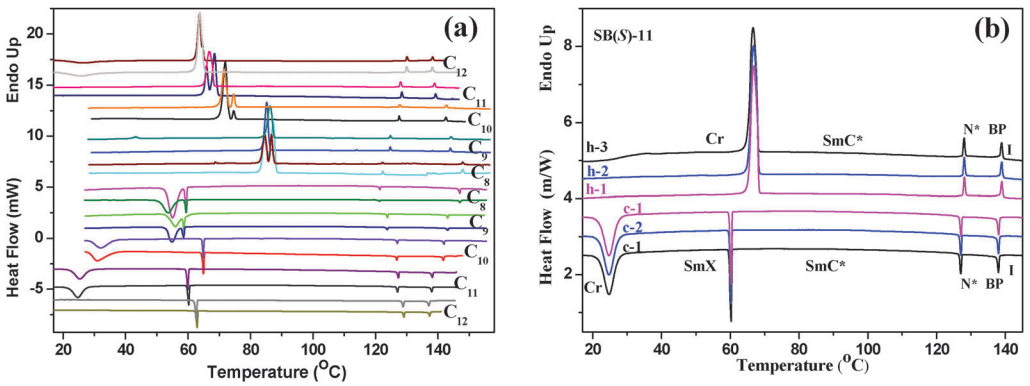

Fig. 3 (a) DSC traces obtained during the first heating–cooling cycles at a rate of 5 °C for all the five pairs of enantiomers; (b) DSC traces recorded for the three successive heating (h-1, h-2 & h-3)–cooling (c-1, c-2 & c-3) cycles at a rate of 5 °C for the mesogen **SB(*S*)-11**; note that the peak positions of all the traces match.

orientation (dark-field of view) implies an orthogonal arrangement of the mesogens with respect to the layer planes. Enthalpy change measured for this transition, which is in the range of 3.9 to 5.8 kJ mol^{-1}, was found to be much higher than those obtained for the I–BP–N* and N*–SmC* transitions. Based on these results it may be appropriate to point out that the SmX phase is a highly ordered smectic phase; we shall discuss about this topic later based on the results of XRD.

Thus, using ordinary (untreated) glass substrates a phase sequence *viz.*, BP–N*–SmC*–SmX was established for all the five pairs of enantiomers synthesized. To corroborate this assignment, all of them were further examined for their optical textural behaviour in glass substrates treated with polyimide and octadecyltriethoxysilane (ODSE) that respectively ensure planar and homeotropic anchoring of mesogens. The platelet texture (as shown in Fig. 2a) was observed for the BP-I/II when substrates treated for either planar or homeotropic geometry were used. Likewise, an uncharacteristic textural pattern, as described before (see Fig. 2b), was seen for the N* phase regardless of the surface treatment employed. When the SmC* phase is formed

from the planar texture of the N* phase, striking fan-shaped domains (batonnets) grow with the simultaneous appearance of equidistant lines (stripes) on the surface of the fans. Given the fact that the SmC* phase is a layered phase formed by chiral molecules, it contains a modulated structure of the director and thus, a striped microscopic texture emerges implying the existence of a helical super structure. A transient textural pattern observed while approaching the transition to the SmC* phase from the planarly aligned N* phase, indicates that the orientation of helix axes of the N* phase perpendicular to the substrate plane whereas that of the SmC* phase remains in the plane of the substrate. Upon cooling the samples from the planar texture of the SmC* phase, a phase transition to the SmX occurs exhibiting a texture having focal-conics, a fan-shaped pattern and polygonal domains, as shown in Fig. 2h. It is well-known that if the helix axis of the SmC* phase is along the direction of light propagation (optic axis) then a grayish/cloudy textural pattern is seen; such a pattern comprises a schlieren texture if the molecular tilt angle is high.[24] Thus, the SmC* phase of the samples held between substrates treated for homeotropic anchoring displayed a cloudy texture as shown in Fig. 2i. Whereas the SmX phase showed a pseudo-isotropic pattern when investigated under the experimental condition mentioned above.

2.2.2. X-ray diffraction. In order to elucidate the structure of the smectic (SmC* and SmX) phases, X-ray measurements were performed on unaligned (powder) samples namely, **SB(*R*)-8** and **SB(*R*)-12**, as representative cases. The XRD experiments were carried out with CuK_α (λ = 0.15418 nm) radiation. The samples under investigation were heated slightly above their isotropization temperature and filled individually into two different Lindemann capillary (1 mm diameter) tubes and both the ends of the tubes were flame sealed. The samples were heated and cooled from their isotropic phase, and the profiles were recorded as a function of temperature in the entire SmC* phase regime. Indeed, comparable diffraction patterns were obtained for both mesogens in their SmC* phase. Fig. 4a and b (red traces) illustrate the typical intensity *versus* diffraction (2θ) profiles obtained for **SB(*R*)-8** (at 110 °C) and **SB(*R*)-12** (125 °C) respectively.

Specifically, the diffractograms obtained at different temperatures exhibited analogous characteristics; while a sharp and intense peak was seen in the small angle region ($0 < 2\theta < 5^\circ$) (see, Fig. 4a and b red traces), the wider angle regime ($2\theta \approx 20^\circ$) contained a weak and diffuse peak (*viz.*, insets of Fig. 4a and b red traces). Indeed, XRD patterns with the single, high-angle diffuse scattering accompanied by a sharp low angle Bragg reflection is typical of a smectic phase wherein the constituent mesogens, being orientationally aligned, form a layered structure with inter-molecular separation within the smectic layer arising due to the liquid-like positional correlation in the smectic layer. Fig. 5 portrays the thermal variation of the layer spacing (d) derived from the low angle Bragg reflections. Table 2 provides spacings d related to the low-angle reflections, wide-angle peak positions and the molecular length (L) of the two mesogens in their most extended form with an all-*trans* conformation of the alkoxy chains; the d/L ratio and the tilt angle (θ) of the mesogens, estimated using the expression $\theta = \cos^{-1}(d/L)$, are also given in the table.

It is clear from the accumulated data that the d-values, ranging between 30.8–32.8 Å for the compound **SB(*R*)-8** and 33.6–34.6 Å for **SB(*R*)-12**, are smaller than the respective estimated all-*trans* (theoretical) molecular length of 3.75 nm and 4.25 nm (see Fig. 6) and accordingly, the d/L ratios are less than one. These results obviously imply either a tilted monolayer arrangement of the molecules with respect to the layer normal direction or interdigitated organization. However, given the fact that d-values are shorter than the fully stretched molecular length,

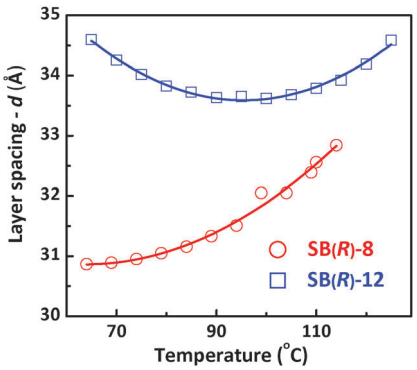

Fig. 5 The layer spacing (d/Å) recorded as a function of temperature in the SmC* phase of the mesogens **SB(*R*)-8** and **SB(*R*)-12**, as representative cases.

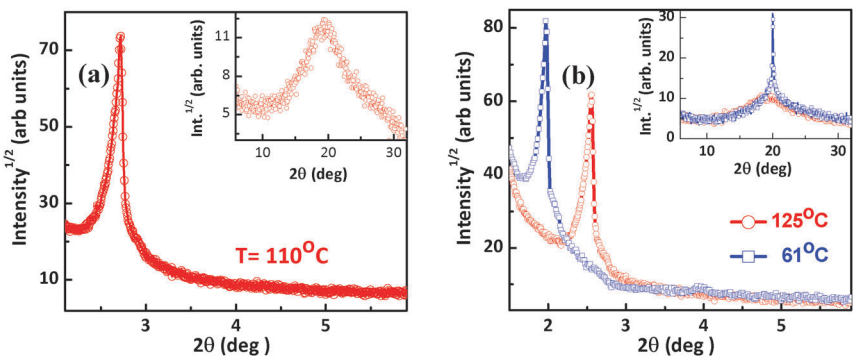

Fig. 4 The low-angle and wide-angle (inset) regions of the XRD patterns obtained for the smectic phases of mesogens: (a) the intensity *vs.* 2θ profile obtained in the SmC* phase of **SB(*R*)-8**; (b) the intensity *vs.* 2θ profiles of the SmC* phase (red traces) and SmX phase (blue traces) belonging to **SB(*R*)-12**.

Table 2 XRD and related data of the SmC* belonging to compounds **SB(*R*)-8** and **SB(*R*)-12**: the spacings (*d*) corresponding to the low-angle reflections, the wide-angle peak positions, the molecular length (*L*) in the most extended form with an all-*trans* conformation of the alkoxy chains, *d*/*L* ratio and tilt angle of the mesogens

Mesogen (*L*/Å)	Temperature/°C	Layer spacing – *d* (low-angle peak position)/Å	Wide-angle peak position/Å	*d*/*L*	Tilt angle (θ) $\theta = \cos^{-1}(d/L)$
SB(*R*)-8 (37.5)	114	32.8	4.58	0.874	29.0
	110	32.6		0.869	29.7
	109	32.4		0.864	30.2
	104	32.05		0.855	31.2
	99	32.1		0.856	31.1
	94	31.5		0.840	32.9
	89	31.3		0.835	33.4
	84	31.2		0.832	33.7
	79	31.0		0.827	34.2
	69	30.89		0.824	34.5
	64	30.86		0.823	34.6
SB(*R*)-12 (42.5)	125	34.6	4.6	0.814	35.5
	120	34.2		0.805	36.4
	115	33.9		0.798	37.1
	110	33.8		0.795	37.3
	105	33.7		0.793	37.5
	100	33.62		0.791	37.7
	95	33.65		0.792	37.6
	90	33.6		0.791	37.7
	85	33.7		0.793	37.5
	80	33.8		0.795	37.3
	75	34.0		0.800	36.9
	70	34.2		0.805	36.4
	65	34.6		0.814	35.5

but longer than a layer spacing of the possible intercalated structure, it is appropriate to consider the lamellar structure under investigation as the SmC* phase where the constituent mesogens tilt from layer to layer about an axis perpendicular to the layer planes yielding a helical structure; this view is strongly substantiated by the observation of a characteristic banded fan-shaped texture as described earlier. As can be seen in Fig. 5 (red-trace), for the mesogen **SB(*R*)-8** the layer spacing decreases almost smoothly upon cooling the phase temperature implying that the tilt angle of the molecules within the smectic layers increases upon lowering the temperature; while for the compound **SB(*R*)-12** the layer spacing decreases first, as expected, and then increases slightly upon cooling the SmC* phase (Fig. 5 blue-trace) which can be attributed to some fine structural variation in the smectic layers. In essence, the XRD study confirms the tilted organization of the mesogens within the smectic layers and thus, supports the presence of the SmC* phase.

Fig. 4b shows the intensity *vs.* 2θ profiles recorded at 61 °C for the SmX phase (blue traces) of mesogen **SB(*R*)-12**; in fact, a virtually identical XRD pattern was obtained at 50 °C. Both the diffractograms obtained at 61 °C and 55 °C comprised a sharp and intense reflection in the low-angle region with the respective spacing being 44.68 Å and 44.73 Å. The occurrence of a sharp low-angle peak suggests a lamellar structure with the layer thickness *d*, which is nearly equal to the theoretical molecular length of 4.25 nm suggesting that the long axes of mesogens (director, *n*) lie along the layer normal, which is supported by the results of a microscopic study; that is, the observation of a fan-shaped texture imply a layered structure, whereas the pseudo-isotropic pattern of the homeotropic alignment, imply an orthogonal organization of mesogens with respect to the smectic layer planes. Interestingly, at wide-angles, both the profiles showed a diffuse and broad-scattering halo with *d* = 4.44 and 4.45 as well as another intense and sharp peak with the spacings of 4.43 and 4.42 Å. The latter reflections of the two profiles are characteristic

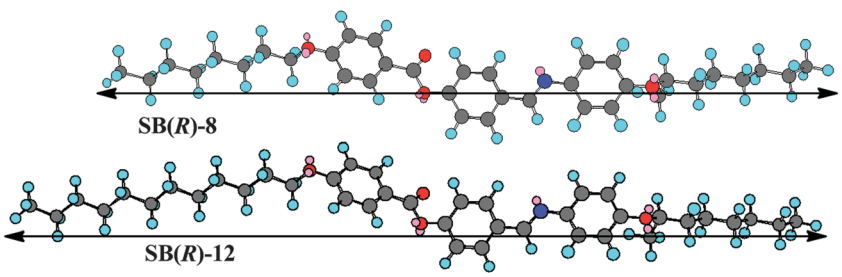

Fig. 6 Energy-minimized ball-and-stick models of the most extended form with an all-*trans* conformation of the alkoxy chains (derived from MM2 of the ChemBioDraw Ultra 12.0) of the **SB(*R*)-8** and **SB(*R*)-12** with respective theoretical molecular lengths of 37.5 Å and 42.5 Å.

of liquid-like order within the smectic planes while the former peaks indicate the additional ordering of the molecules within the layers. Seemingly, the experimental data available at this point of time are inadequate to figure out the explicit structure of the SmX phase although XRD studies point to a possible tilted hexatic phase.

We now return to the temperature dependence of the layer spacing (tilt angle) in the SmC* phase. Both the materials show large tilt angle values characteristic of systems exhibiting a direct transition from the N/N* to SmC/SmC* phase. The temperature dependence presents an important difference between the two compounds. While the shorter homologue, **SB(*R*)-8**, has monotonically decreasing layer spacing (an increasing tilt angle) typical of the SmC* phase, the longer homologue has an anomalous behaviour. Upon cooling the sample, the layer spacing decreases up to a certain temperature and then reverses its trend (see Fig. 5). Such an unusual feature is not common in materials presenting the N*–SmC* transition. Even in the more commonly occurring SmA–SmC* transition systems only a few materials are known with such a phenomenon. The SmA phase of such materials has been identified to be of the technologically important de Vries.[25] A possible explanation for the trend reversal of the layer spacing (or tilt angle) is that the negative thermal expansion of the layer structure (owing to the stretching of the terminal alkyl chains) counterbalances the decrease in the layer spacing due to the tilted nature of the phase. A second possibility is that the reversal is a pretransition variation upon approaching the low temperature SmX phase. In fact, when the low temperature phase is a tilted hexatic such a feature is indeed seen.[26]

2.2.3. Electrical switching study. As discussed before, the helical structure of the SmC* phase stems as a result of a gradual change in molecular tilt direction from layer to layer, about an axis vertical to the layer planes. The reduced C_2 symmetry and tilting of the constituent chiral mesogens result in P_s in the plane of each layer, which, however, averages out to zero due to the helical structure. As is well known, to obtain a macroscopic P_s the helix needs to be unwound by application of an electric field. Thus, to investigate the polar properties of the SmC* phase electric field experiments were carried out on mesogens **SB(*R*)-8** and **SB(*R*)-12** as representative cases. The cells fabricated using two ITO coated glass plates pre-treated with a polyimide solution, and rubbed unidirectionally, which enable the homogeneous orientation of the mesogens, were used for the study. The samples were filled into cells in their isotropic phase through capillary action and cooled slowly to the mesophase. A low frequency AC triangular-wave voltage was applied and slowly increased. At a voltage of 46.8 V_{rms} and a frequency of 20 Hz, the SmC* phase of the sample **SB(*R*)-8** exhibited a profile comprising a single polarization current peak for each half period indicating a ferroelectric switching behaviour. As a representative case the current response profile obtained at 90 °C is shown Fig. 7a. The textural change observed under POM in the field on-state and off-state as are presented in Fig. 7c, d and b respectively. The macroscopic P_s value, obtained by integrating the area under the peaks, was found to be ~108 nC cm^{-2}. Likewise, by applying a triangular-wave electric field of about 18.5 V_{rms} and a frequency of 20 Hz, the mesophase of **SB(*R*)-12** exhibited a single polarization current peak with P_s = 123.8 nC cm^{-2}; switching current response trace and optical textures obtained under these experimental conditions are shown in Fig. 7e and f, h respectively. It must be mentioned here that the switching peak of the SmC* phase vanishes completely when the samples are heated to their isotropic melt implying the origin of switching from the mesophase

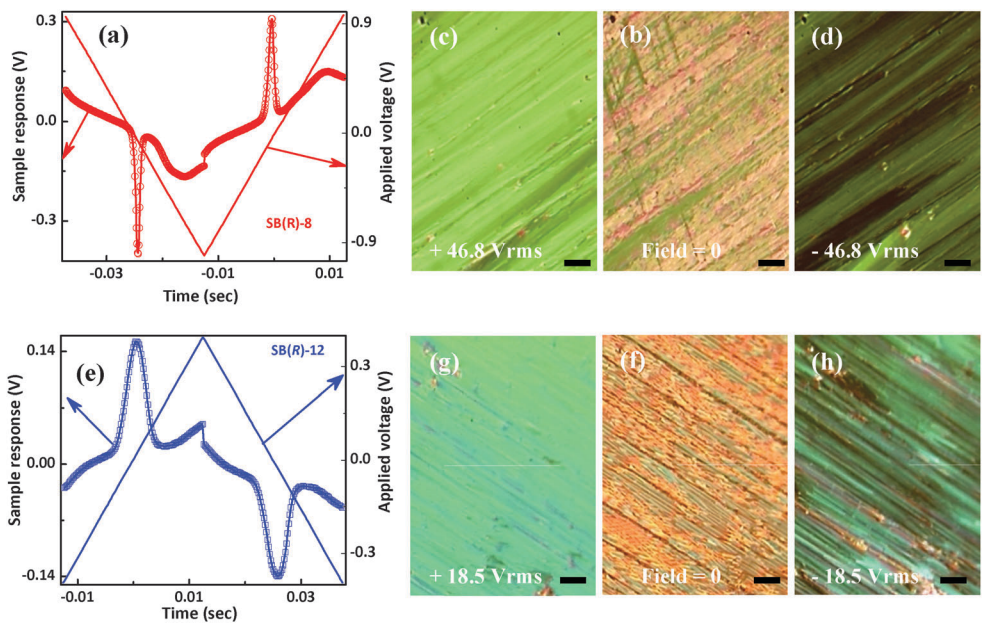

Fig. 7 Switching current response peaks obtained upon applying a triangular-wave filed for the SmC* phase of mesogens **SB(*R*)-8** (90 °C; 46.8 V_{rms}, 20 Hz; 09 kΩ; P_s = 108 nC cm^{-2}) (a) and **SB(*R*)-12**, (70 °C; 18.5 V_{rms}, 20 Hz; 09 kΩ; P_s = 123.8 nC cm^{-2}) (e). Microphotographs of the microscopic textural changes observed under the applied electric field (c, d & g, h) and in the absence of field (b & f) (bar: 100 μm).

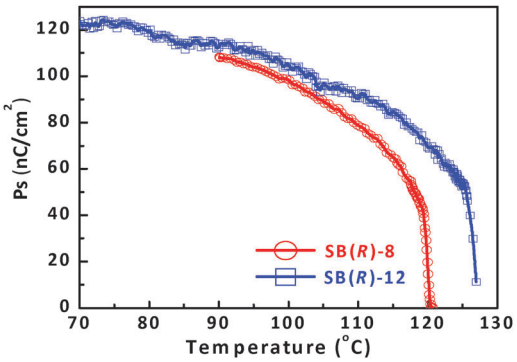

Fig. 8 A profile showing the temperature dependence of the P_s in the SmC* phase of compounds **SB(*R*)-8** (red-trace) and **SB(*R*)-12** (blue-trace).

but not from the ionic impurities. Fig. 8 illustrates the temperature dependence of P_s where it can be seen that with increasing temperature the P_s decreases progressively and disappears across the SmC*–N* transition.

Hence, the foregoing experimental results confirm the ferroelectric nature of the chiral smectic phase. It may also be mentioned here that these samples were found to be very stable even after repetitive application of the electric field.

2.2.4. UV-vis and circular dichroism spectroscopic studies. Considering the fact that the present series of compounds are chiral and possess light absorbing groups (chromophores), they were investigated for their photophysical and chirooptical properties with the aid of UV-vis absorption and circular dichroism (CD) spectroscopic techniques, respectively. The solution UV-vis spectra ($\sim 3 \times 10^{-3}$ M in CH_2Cl_2; cell length = 1 mm) of all the mesogens were found to be virtually identical; as representative cases, the spectra obtained for all the (*S*)-enantiomers are shown in Fig. 9. Seemingly, each spectrum comprises two peaks at ~275 and 340 nm which can be assigned to π–π* and n–π* transitions, respectively. However, CD signals of the corresponding wavelengths were found to be non-existent (zero) in the solution CD spectra of the samples implying the absence of chiral aggregations and thus, macroscopic helical ordering.

CD spectroscopy, wherein the circular dichroism is measured as a function of wavelength, has been demonstrated as a powerful technique to study the chirooptical behavior of the N* [11,13,15,27] and SmC* [20b,28] phases. As is well-known, in a well-aligned homogeneous orientation (the Grandjean texture), the director of the N* phase rotates in a helical fashion around a perpendicular axis with a pitch *p*; depending upon the chirality of the constituent mesogens the pitch value ranges from hundreds of nanometers (for strongly chiral mesogens) to hundreds of micrometers. The helix-sense or handedness (left or right) of the N* phase describes the direction in which rotation of the director occurs from one layer to another. The CD spectral study helps in figuring out handedness as the circularly polarised light (CPL), being a chiral system, interacts differently with the N* phase formed by the two enantiomers of a chiral compound. That is, the N* phase shows CD at a given wavelength where the incident light is resolved into its two CP components namely, left and right; at this wavelength, depending upon the natural helical sense of the phase formed by a particular enantiomer, the CPL of a particular handedness is completely reflected while its counterpart is transmitted. In other words the rotation of the reflected CPL agrees with the screw sense of the N* helix while the transmitted light possesses opposite handedness. Thus, the handedness (screw sense) of the helical array of the N* or SmC* phase formed by the enantiomers (mirror-image isomers) should be opposite to each other; consequently, the enantiomeric pairs display mirror image signals in CD spectra. In order to figure out such chirooptical properties, the N* and SmC* phases formed by a pair of enantiomers, **SB(*R*)-9** and **SB(*S*)-9**, were subjected to a CD spectroscopic study, as representative cases.

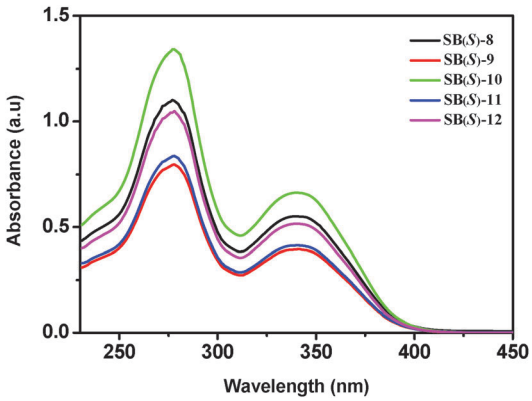

Fig. 9 UV-vis spectrum recorded for the dilute (dichloromethane) solutions of the (*S*)-enantiomers.

The CD experiments were carried out using thin films of the above mesogens contained between two quartz plates. The samples were heated slightly (5 °C) above their isotropic melt temperature and hard-pressed; this process was repeated a couple of times, which ensures the spreading of the sample thinly and evenly. In fact, such thin films were found to be crucial to work within the upper limits (saturation) of measurement where the stronger CD signals were found to be out of the measurable range of the CD instrument. This means that the cells of known thickness could not be used and hence, the present CD experiments are qualitative. The samples, such as above, were cooled slowly from their isotropic melt and mechanically sheared repeatedly when the N* phase appears. Thereby, the N* phase attains the Grandjean texture where the helix lies normal to the quartz plates that reflects the incident light readily. While cooling the samples, the CD spectra were recorded in the entire thermal range of both N* and SmC* phases. As shown in Fig. 10, both the phases of the samples displayed the CD signals, as expected, where the intensity of the peaks increases with decrease in temperature; the position, sign and intensity of the CD bands obtained as a function of temperature for the enantiomeric pairs are given in Table 3. It must be noted here that, the CD phenomenon, when compared to the N* phase, was found to be immeasurably small (nearly zero) in the spectra of the isotropic melt implying the origin of the CD activity from the chiral LC structure but not from the molecular chirality. Further, the presence of CD peaks in both the LC phases of the samples was validated by obtaining the spectra by 90° in-plane rotation of

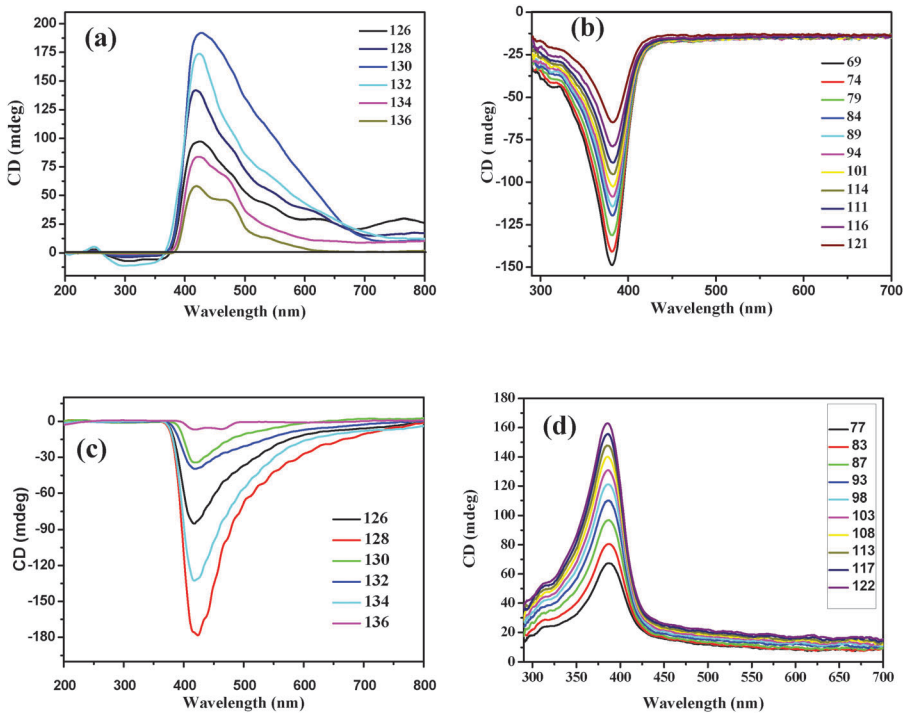

Fig. 10 CD spectra recorded as a function of temperature in the N* (a and c) and SmC* (b and d) phases exhibited by the enantiomer **SB(*R*)-9** and **SB(*S*)-9**.

the samples; the spectra were found to be nearly identical to those obtained in the pristine orientation. This infers that the CD signal is not arising from the possible linear dichroism (LD) artifact. Further, the CD instrument used has a built in facility to measure the LD directly. Thus, both LC phases were subjected to direct LD measurement where the activity was found to be zero, as contemplated.

As can be seen in Fig. 10a–d, the CD spectra obtained for the N* and SmC* phases of enantiomers **SB(*R*)-9** and **SB(*S*)-9** exhibit an excellent mirror-image relationship over their entire thermal range. From the Fig. 10a it can be specifically seen that the CD spectra recorded at different temperatures for the N* phase of an enantiomer **SB(*R*)-9** exhibit a broad positive peak with the λ value ranging between 419–426 nm (Table 3) which corresponds to the absorption wavelength of n–π* transition of the chiral chromophore; whereas its counterpart N* phase, belonging to the (*S*)-enantiomer, **SB(*S*)-9**, displays a negative signal (λ = 418–430 nm; see Fig. 10c and Table 3), as expected. It is a very widespread conception that[29] the positive CD band corresponds to a right-handed screw sense of a helicoidal structure. Thus, the helix sense of the N* phase formed by **SB(*R*)-9**, exhibiting a positive CD peak, is right-handed, whereas it is left-handed for the N* phase of **SB(*S*)-9** as it shows a negative signal. The temperature dependence of the CD spectra recorded in the entire SmC* phase range of the enantiomers **SB(*R*)-9** and **SB(*S*)-9** are shown in Fig. 10b and d, respectively, where the CD peaks obtained from helical structures of opposite handedness are perfect mirror images. This clearly implies the mirror-image chiral structures where the handedness (screw sense) of the helical array of the SmC* phase formed by the two enantiomers (mirror-image isomers) are opposite to each other. However, it is interesting to note that the CD peak obtained in the SmC* phase of **SB(*R*)-9** is opposite (−ve) (Fig. 10b) when compared to that of the +ve CD band seen for the N* phase (Fig. 10a) of the same sample under identical experimental conditions; thus, the sense of the helix in the N* phase is right-handed while it is left-handed in the case of the SmC* phase. Similarly, CD bands are positive (Fig. 10d) and negative (Fig. 10c) for the SmC* and N* phases respectively formed by an enantiomer **SB(*S*)-9**. These results show that the SmC* and N* structures derived from an enantiomer possess opposite helix-sense. That is, the reversal of the helix-sense (from right to left and *vice versa*) occurs during the N* to SmC* phase transition. This is the first time that such an observation has been made where the screw sense of the helical array of the N* phase and the SmC* phase of an enantiomer is opposite.

3. Summary

Ten new three-ring rod-like chiral compounds, especially five pairs of enantiomers, have been synthesized and evaluated for mesomorphism and optical properties. Each pair of enantiomers consists of (*R*)-2-octyloxy and (*S*)-2-octyloxy chains at one end while the other terminus is substituted with an *n*-alkoxy tail. Thermal investigations reveal an identical mesomorphic behavior of all the five pairs of enantiomers implying that the alteration in the length of the *n*-alkoxy tail has no effect on the observed LC phase sequence such as BP-I/II–N*–SmC*–SmX. However, the transition temperatures and thus, thermal width of the N* and SmC* mesophases show dependence on this variation. The temperature range of the SmC* phase widens when the

Table 3 CD spectroscopic data obtained in N* and SmC* phases as a function of temperature for the enantiomers **SB(*R*)-9** and **SB(*S*)-9**

Compounds	Chiral LC phase	Temperature (°C)	CD	
			λ_{max}/nm	CD (mdeg)
SB(*R*)-9	N*	126	426	+97
		128	419	+142
		130	426	+192
		132	424	+174
		134	423	+84
		136	419	+58
SB(*S*)-9	N*	126	418	−85
		128	424	−178
		130	419	−34
		132	419	−40
		134	418	−133
		136	430	−18
SB(*R*)-9	SmC*	69	382	−149
		74	382	−141
		79	382	−131
		84	382	−120
		89	382	−114
		94	383	−109
		101	383	−103
		114	383	−95
		112	382	−88
		116	383	−79
		121	383	−65
SB(*S*)-9	SmC*	77	386	+163
		83	386	+156
		87	385	+148
		93	386	+140
		98	387	+131
		103	386	+121
		108	387	+110
		113	387	+97
		117	388	+81
		122	388	+67

length of the *n*-alkoxy tail increases. In fact, the influence of this parameter is prominently seen in the isotropization temperatures, which decreases with an increase in the chain length. The occurrence of the technologically important SmC* phase, over the thermal width of 20–55 °C, has been established unambiguously with the help of conventional techniques such as microscopic, calorimetric and XRD. The electro-optical experiments carried out confirm the ferroelectric switching behavior of the SmC* phase; the calculated P_s value was found to be over 100 nC cm^{-2}. Notably, these mesogens, being Schiff bases, remain intact even after subjecting them to repetitive electric switching experiments; indeed, a similar observation was made during the repetitive heating–cooling cycles of the microscopic and calorimetric studies. The solution-state UV-vis spectra (in CH_2Cl_2) of the compounds show two peaks at ~275 and 340 nm due to π–π* and n–π* transitions, respectively; CD bands of the corresponding wavelengths were found to be totally absent. However, the thin films of the samples show strong CD signals in the entire temperature range of both N* and SmC* phases confirming the chromophores of the mesogens being in a macroscopic chiral environment; in other words, the inherent helical structure of the phases is evidenced formally. The N* or SmC* phase formed by enantiomeric mesogens showed macroscopic helices of opposite handedness, as expected. The measurements also confirmed that the handedness of helices of the N* and SmC* phases of an enantiomer remain opposite. To the best of our knowledge this is the first observation that during the phase transition from the N* phase to SmC* phase the reversal of the helix from left (right) to right (left) handedness occurs.

4. Experimental

4.1. General information

All chemicals obtained from overseas/local companies were used as received. All chromatographic solvents were distilled prior to use and other solvents were purified following the standard protocols. To monitor the progress and completion of reactions, and also to assess the purity of the compounds thin layer chromatography (TLC) was used; for this purpose, aluminium sheets pre-coated with silica gel (Merck, Kieselgel60, F254) were used. Silica gel (60–120, 100–200 and 230–400 mesh), neutral aluminium oxide and basic aluminium oxide were used as stationary phases in the column chromatography technique. All intermediates and target compounds were structurally characterized primarily with the help of IR, NMR and FTIR spectroscopic techniques. ^{1}H and ^{13}C NMR spectra of the compounds in $CDCl_3$ were recorded using a Bruker AMX-400 (400 MHz) spectrometer. For ^{1}H NMR spectra, the chemical shifts are reported in parts per million (ppm) relative to tetramethylsilane (TMS) as an internal standard. Coupling constants (J) are given in Hz. IR spectra were recorded on a FT-IR spectrometer; the spectral positions are given in the wave number (cm^{-1}) unit. IR spectra were recorded on a PerkinElmer Spectrum 1000 FT-IR spectrometer. Electronic absorption (UV-vis) spectra were recorded with the help of Perkin Elmer's, Lambda 20 UV-vis spectrometer. Elemental microanalysis was performed using a Eurovector E300 elemental analyzer. Mass spectra were recorded on a JEOL JMS-600H spectrometer (Tokyo, Japan) in FAB+ mode using 3-nitrobenzyl alcohol as a liquid matrix. Specific rotation of the compounds was measured using a Rudolph AUTOPOL IV Automatic Polarimeter. CD spectra were recorded with the aid of a Jasco J-810 spectropolorimeter. Molecular lengths of target mesogens were determined (in Å) from the energy minimized (all-*trans*) structure deduced from ChemBio3D Ultra 12.0 programme.

The thermal behavior of the compounds were examined with the help of an optical polarizing microscope (Olympus BX50; Model BX50F4) equipped with a programmable hot stage (Mettler FP90) and differential scanning calorimeter (DSC) (Perkin-Elmer Diamond DSC with the PC system operating on Pyris software) apriorically calibrated using pure indium as a standard. The phase transition temperatures and associated enthalpies were determined from DSC traces recorded at a scanning rate of 5 °C min^{-1}. X-Ray diffraction studies were carried on powder samples in Lindemann capillaries with CuK_α (λ = 0.15418 nm) radiation using the PANalytical X'Pert PRO MP X-ray diffractometer consisting of a focusing elliptical mirror and a fast resolution detector (PIXCEL).

4.2. Synthesis and characterization

4.2.1. General procedure for the synthesis of (*R*)- and (*S*)-1-nitro-4-(octan-2-yloxy)benzenes (I and III). To a cooled (10–15 °C) and magnetically well-stirred solution of 4-nitrophenol (7.2 mmol, 1 eq.), (*R*)-2-octanol or (*S*)-2-octanol, triphenylphosphine (8.6 mmol, 1.2 eq.) in dry THF, diisopropylazo dicarboxylate was added drop wise over a period of 5 min. under an argon atmosphere. The reaction mixture was allowed to attain room temperature (RT) and stirred for 12 hours. The solvent was removed *in vacuo* and extracted with dichloromethane (CH_2Cl_2), washed with 5% NaOH (25 mL × 2) solution, water, brine and dried over anhydrous Na_2SO_4. Evaporation of solvent *in vacuo* furnished crude oil, which was purified by column chromatography using silica gel (60–120 mesh). Elution with a mixture of 10% CH_2Cl_2–hexanes, afforded the yellow oil.

*(R)-1-Nitro-4-(octan-2-yloxy)benzene (**I**).* R_f = 0.6 (20% EtOAc–hexane); a pale yellow liquid; yield: 1.66 g (92%); IR (KBr pellet): ν_{max} in cm^{-1} 3451, 3085, 2932, 2859, 2447, 1910, 1607, 1592, 1513, 1466, 1380, 1340, 1296 and 1261; ^1H NMR (400 MHz, $CDCl_3$): δ 8.19 (d, J = 9.6 Hz, 2H, Ar), 6.92 (d, J = 9.6 Hz, 2H, Ar), 4.50 (m, 1H, –O–CH–) and 1.80–0.86 (m, 16H, 2 × CH_3, 5 × CH_2).

*(S)-1-Nitro-4-(octan-2-yloxy)benzene (**III**).* R_f = 0.59 (20% EtOAc–hexane); a pale yellow liquid; yield: 1.65 g (91%); IR (KBr pellet): ν_{max} in cm^{-1} 3451, 3085, 2932, 2858, 2447, 1909, 1592, 1513, 1494, 1465, 1380, 1340, 1296 and 1261; ^1H NMR (400 MHz, $CDCl_3$): δ 8.19 (d, J = 9.2 Hz, 2H, Ar), 6.92 (d, J = 9.2 Hz, 2H, Ar), 4.51 (m, 1H, –O–CH–) and 1.80–0.86 (m, 16H, 2 × CH_3, 5 × CH_2).

4.2.2. General procedure for the synthesis of (*R*)- and (*S*)-4-(octan-2-yloxy)anilines (II and IV). (*R*)-(**I**) or (*S*)-1-nitro-4-(octan-2-yloxy)benzene (**III**) (0.1 g, 0.4 mmol, 1 eq.) was dissolved in dry THF and 10% Pd–C (0.01 g) was added. The resultant reaction mixture was degassed and stirred under H_2 gas for 4 h at rt. The reaction mixture was filtered, concentrated and the liquid obtained was purified by flash column chromatography using basic alumina as a stationary phase and 20% EtOAc–hexanes as an eluent.

*(R)-4-(Octan-2-yloxy)aniline (**II**).* R_f = 0.23 (10% EtOAc–hexane); a yellow liquid; yield: 0.081 g (92%); IR (KBr pellet): ν_{max} in cm^{-1} 3358, 3222, 3036, 2957, 2929, 2857, 1624, 1509, 1463, 1376 and 1232; ^1H NMR (400 MHz, $CDCl_3$): δ 6.74 (d, J = 8.8 Hz, 2H, Ar), 6.63 (d, J = 8.8 Hz, 2H Ar), 4.19 (m, 1H, –O–CH–), 3.42 (brs, 2H, –NH_2) and 1.73–0.86 (m, 16H, 2 × CH_3, 5 × CH_2); ^{13}C NMR (100 MHz): 151.20, 140.04, 117.84, 116.34, 75.23, 36.55, 31.78, 29.28, 25.53, 22.56, 19.83 and 14.03.

*(S)-4-(Octan-2-yloxy)aniline (**IV**).* R_f = 0.24 (20% EtOAc–hexane); a yellow liquid; yield: 0.08 g (91%); IR (KBr pellet): ν_{max} in cm^{-1} 3357, 3222, 2956, 2829, 2857, 1854, 1624, 1508, 1465, 1376 and 1233; ^1H NMR (400 MHz, $CDCl_3$): δ 6.74 (d, J = 8.8 Hz, 2H, Ar); 6.63 (d, J = 8.8 Hz, 2H Ar); 4.19 (m, 1H, –O–CH–), 3.40 (brs, 2H, –NH_2) and 1.74–0.86 (m, 16H, 2 × CH_3, 5 × CH_2); ^{13}C NMR (100 MHz): 150.8, 139.6, 117.53, 115.9, 74.9, 36.12, 31.35, 29.22, 25.1, 22.12, 19.40 and 13.58.

4.2.3. General procedure for the synthesis of 4-(*n*-alkoxy)-benzaldehydes (Va–e). A mixture of 4-hydroxybenzaldehyde (1 g, 8.19 mmol, 1 eq.), *n*-alkylbromide (9.01 mmol, 1.1 eq.), anhydrous K_2CO_3 (9.01 mmol, 1.1 eq.) and DMF was heated in an inert atmosphere for 12 h. After cooling, the reaction mixture was poured into ice-cold water and the product was extracted with dichloromethane (50 mL × 3). The combined organic layers were washed with cold aqueous (5%) NaOH solution (25 mL × 3), water (25 mL × 3), brine and dried over anhydrous Na_2SO_4. The solvent was removed *in vacuo* and the crude product obtained was purified by column chromatography on silica gel (100–200 mesh) using 10% EtOAc–hexanes as an eluent.

Va. R_f = 0.51 (30% CH_2Cl_2–hexanes); a colorless liquid; yield: 1.54 g (80.0%); IR (KBr pellet): ν_{max} in cm^{-1} 2959, 2873, 1695, 1601, 1231, 1128 and 1113; ^1H NMR (400 MHz, $CDCl_3$): δ 9.88 (s, 1H, –CHO), 7.84 (d, J = 6.8 Hz, 2H, Ar), 7.01 (d, J = 6.8 Hz, 2H, Ar), 4.05 (t, J = 6.8 Hz, 2H, –OCH_2), 1.85–1.28 (m, 12H, 6 × CH_2) and 0.90 (t, J = 6.8 Hz, 3H, –CH_3); MS (FAB+): m/z for $C_{15}H_{23}O_2$ (M + 1), calculated: 235.2, found: 235.2.

Vb. R_f = 0.51 (30% CH_2Cl_2–hexanes); a colorless liquid; yield: 1.67 g (82.0%); IR (KBr pellet): ν_{max} in cm^{-1} 2959, 2877, 1699, 1601, 1259, 1160 and 1112; ^1H NMR (400 MHz, $CDCl_3$): δ 9.9 (s, 1H, –CHO), 7.82 (d, J = 8.4 Hz, 2H, Ar), 6.99 (d, J = 8.8 Hz, 2H, Ar), 4.04 (t, J = 6.4 Hz, 2H, –OCH_2), 1.88–1.31 (m, 14H, 7 × CH_2) and 0.87 (t, J = 6.6 Hz, 3H, –CH_3); MS (FAB+): m/z for $C_{16}H_{25}O_2$ (M + 1), calculated: 249.2, found: 249.2.

Vc. R_f = 0.52 (30% CH_2Cl_2–hexanes); a colorless liquid; yield: 1.82 g (85.0%); IR (KBr pellet): ν_{max} in cm^{-1} 2926, 2855, 1670, 1215, 1160 and 1109; ^1H NMR (400 MHz, $CDCl_3$): δ 9.88 (s, 1H, –CHO), 7.84 (d, J = 8.8 Hz, 2H, Ar), 7.01 (d, J = 6.8 Hz, 2H, Ar), 4.05 (t, J = 6.4 Hz, 2H, –OCH_2), 1.83–1.30 (m, 16H, 8 × CH_2) and 0.90 (t, J = 6.8 Hz, 3H, –CH_3); MS (FAB+): m/z for $C_{17}H_{26}O_2$, calculated: 262.2, found: 262.5.

Vd. R_f = 0.52 (30% CH_2Cl_2–hexanes); a colorless liquid; yield: 1.76 g (78.0%); IR (KBr pellet): ν_{max} in cm^{-1} 2962, 2877, 1700, 1606, 1262, 1164 and 1113; ^1H NMR (400 MHz, $CDCl_3$): δ 9.9 (s, 1H, –CHO), 7.82 (d, J = 8.4 Hz, 2H, Ar), 6.99 (d, J = 8.8 Hz, 2H, Ar), 4.04 (t, J = 6.4 Hz, 2H, –OCH_2), 1.88–1.31 (m, 18H, 9 × CH_2) and 0.87 (t, J = 6.6 Hz, 3H, –CH_3); MS (FAB+): m/z for $C_{18}H_{28}O_2$, calculated: 276.2, found: 276.6.

Ve. R_f = 0.53 (30% CH_2Cl_2–hexanes); a colourless liquid; yield: 2.01 g (85.0%); IR (KBr pellet): ν_{max} in cm^{-1} 2927, 2855, 1694, 1230, 1160 and 1110; ^1H NMR (400 MHz, $CDCl_3$): δ 9.88 (s, 1H, –CHO), 7.83 (d, J = 6.8 Hz, 2H, Ar), 7.00 (d, J = 6.8 Hz, 2H, Ar), 4.04 (t, J = 6.4 Hz, 2H, –OCH_2), 1.88–1.31 (m, 20H, 10 × CH_2) and 0.87 (t, J = 6.6 Hz, 3H, –CH_3); MS (FAB+): m/z for $C_{20}H_{30}O_2$, calculated: 290.1, found: 290.6.

4.2.4. General procedure for the synthesis of 4-(*n*-alkoxy)-benzoic acids (VIa–e). A solution of 4-(*n*-alkoxy)benzaldehyde (**Va–e**) (1 g) in dry acetone 20 mL was cooled to 0 °C and Jones reagent (1.75 g of CrO_3 dissolved in 5 mL water and 2 mL H_2SO_4) was added slowly maintaining the temperature below 5 °C. The reaction mixture was stirred at RT for 1 h and poured

into cold water. A colourless precipitate obtained was filtered, washed with water thoroughly and air dried. The crude material was recrystallized from hexanes to get the pure product.

VIa. R_f = 0.19 (20% EtOAc–hexanes); a colourless solid; yield: 1.27 g (84%); phase sequence: Cr 76.6 °C [60.5 J g^{-1}] Cr_1 101.3 [44.9] SmC 107.5 [4.9] N 147.9 [7.4] I; IR (KBr pellet): ν_{max} in cm^{-1} 2919, 2849, 1775, 1686, 1606, 1578, 1256 and 1169; ^{1}H NMR (400 MHz, $CDCl_3$): δ 8.06 (d, J = 8.8 Hz, 2H, Ar), 6.94 (d, J = 9.2 Hz, 2H, Ar), 4.04 (t, J = 6.6 Hz, 2H, $-OCH_2$), 1.84–1.23 (m, 12H, 6 × CH_2) and 0.91 (t, J = 6.8 Hz, 3H, $-CH_3$); MS (FAB+): m/z for $C_{15}H_{22}O_3$, calculated: 250.2, found: 250.3.

VIb. R_f = 0.19 (20% EtOAc–hexanes); a colourless solid; yield: 1.36 g (78%); Cr 94.6 °C [124.5 J g^{-1}] SmC 117.2 [6.3] N 143.5 [6.4] I; IR (KBr pellet): ν_{max} in cm^{-1} 2918, 2851, 1774, 1686, 1606, 1578, 1257 and 1169; ^{1}H NMR (400 MHz, $CDCl_3$): δ 8.06 (d, J = 9.2 Hz, 2H, Ar), 6.94 (d, J = 8.8 Hz, 2H, Ar), 4.04 (t, J = 6.6 Hz, 2H, $-OCH_2$), 1.84–1.28 (m, 14H, 7 × CH_2) and 0.90 (t, J = 6.8 Hz, 3H, $-CH_3$); MS (FAB+): m/z for $C_{16}H_{24}O_3$, calculated: 264.2, found: 265.1.

VIc. R_f = 0.19 (20% EtOAc–hexanes); a colourless solid; yield: 1.23 g (86%); Cr 86.1 °C [77.1 J g^{-1}] Cr_1 96 [40.8] SmC 121.6 [5.1] N 141.1 [6.6] I; IR (KBr pellet): ν_{max} in cm^{-1} 2918, 2851, 1774, 1686, 1605, 1578, 1257 and 1170; ^{1}H NMR (400 MHz, $CDCl_3$): δ 8.06 (d, J = 8.8 Hz, 2H, Ar), 6.94 (d, J = 9.2 Hz, 2H, Ar), 4.04 (t, J = 6.6 Hz, 2H, $-OCH_2$), 1.84–1.28 (m, 16H, 8 × CH_2) and 0.90 (t, J = 7 Hz, 3H, $-CH_3$); MS (FAB+): m/z for $C_{17}H_{26}O_3$, calculated: 278.2, found: 278.5.

VId. R_f = 0.19 (20% EtOAc–hexanes); a colourless solid; yield: 1.37 g (77%); Cr 97.2 °C [129 J g^{-1}] SmC 127.1 [6] N 139.2 [6.4] I; IR (KBr pellet): ν_{max} in cm^{-1} 2918, 2849, 1772, 1687, 1606, 1579, 1256 and 1170; ^{1}H NMR (400 MHz, $CDCl_3$): δ 8.06 (d, J = 8.8 Hz, 2H, Ar), 6.94 (d, J = 9.2 Hz, 2H, Ar), 4.04 (t, J = 6.6 Hz, 2H, $-OCH_2$), 1.84–1.27 (m, 18H, 9 × CH_2) and 0.90 (t, J = 7 Hz, 3H, CH_3); MS (FAB+): m/z for $C_{18}H_{28}O_3$, calculated: 292.2, found: 293.5.

VIe. R_f = 0.19 (20% EtOAc–hexanes); a colourless solid; yield: 1.25 g (84%); Cr 95.1 °C [119.9 J g^{-1}] SmC 132.6 [7.7] N 139.1 [6.7] I IR (KBr pellet): ν_{max} in cm^{-1} 2919, 2851, 1774, 1686, 1605, 1578, 1256 and 1169; ^{1}H NMR (400 MHz, $CDCl_3$): δ 8.05 (d, J = 9.2 Hz, 2H, Ar), 6.94 (d, J = 8.8 Hz, 2H, Ar), 4.04 (t, J = 6.6 Hz, 2H, $-OCH_2$), 1.84–1.27 (m, 20H, 10 × CH_2) and 0.90 (t, J = 6.8 Hz, 3H, $-CH_3$); MS (FAB+): m/z for $C_{19}H_{30}O_3$, calculated: 306.2, found: 307.5.

4.2.5. General procedure for the synthesis of 4-formylphenyl 4-(*n*-alkoxy)benzoates VIIa–e. 4-(*n*-Alkoxy)benzoic acid (**VIa–e**) (3.9 mmol, 1 eq.) and 4-hydroxybenzaldehyde (3.9 mmol, 1 eq.) were dissolved in dry THF and stirred under a nitrogen atmosphere for some time. After the addition of DCC (4.7 mmol, 1.2 eq.) and a catalytic amount of DMAP, the reaction mixture was stirred at RT for 48 h. The precipitated dicyclohexylurea was filtered off and the solvent was removed *in vacuo*. The solid substance obtained was purified by column chromatography on silica gel (230–400 mesh) using 10% EtOAc–hexanes as an eluent.

VIIa. R_f = 0.29 (10% EtOAc–hexane); a colourless solid; yield: 0.692 g (89%); m.p = 66.1 °C; IR (KBr pellet): ν_{max} in cm^{-1} 2933, 2854, 1731, 1694, 1602, 1581, 1510, 1468, 1420, 1396 and 1306 cm^{-1}, ^{1}H NMR (400 MHz, $CDCl_3$): δ 10.02 (s, 1H, Ar-CHO), 8.14 (d, 2H, J = 8.8 Hz, Ar), 7.97 (d, J = 8.8 Hz, 2H, Ar), 7.41 (d, J = 8.4 Hz, 1H, Ar), 6.99 (d, J = 9.2 Hz, 2H, Ar), 4.06 (t, J = 6.6 Hz, 2H, $-OCH_2$) and 1.86–0.91 (m, 15H, 1 × CH_3, 6 × CH_2); MS (FAB+): m/z for $C_{22}H_{26}O_4$, calculated: 354.2, found: 355.2.

VIIb. R_f = 0.30 (10% EtOAc–hexane); a colourless solid; yield: 0.700 g (81%); m.p = 67.4 °C; IR (KBr pellet): ν_{max} in cm^{-1} 2918, 2851, 1737, 1698, 1603, 1580, 1510, 1471, 1422, 1397 and 1310 cm^{-1}; ^{1}H NMR (400 MHz, $CDCl_3$): δ 10.02 (s, 1H, Ar-CHO), 8.14 (d, J = 8.8 Hz, 2H, Ar), 7.97 (d, J = 8.4 Hz, 2H, Ar), 7.41 (d, J = 8.4 Hz, 2H, Ar), 6.99 (d, J = 8.8 Hz, 2H, Ar), 4.06 (t, J = 6.4 Hz, 2H, $-OCH_2$) and 1.86–0.87 (m, 17H, 1 × CH_3, 7 × CH_2); MS (FAB+): m/z for $C_{23}H_{28}O_4$, calculated: 368.2, found: 368.7.

VIIc. R_f = 0.28 (10% EtOAc–hexane); a colourless solid; yield: 0.687 g (83%); m.p = 71.8 °C; IR (KBr pellet): ν_{max} in cm^{-1} 2912, 2849, 1737, 1698, 1605, 1580, 1511, 1469, 1422, 1391 and 1270 cm^{-1}; ^{1}H NMR (400 MHz, $CDCl_3$): δ 10.02 (s, 1H, Ar-CHO), 8.15 (d, J = 8.8 Hz, 2H, Ar), 7.97 (d, J = 8.8 Hz, 2H, Ar), 7.41 (d, J = 8.4 Hz, 2H, Ar), 6.99 (d, J = 9.2 Hz, 2H, Ar), 4.06 (t, J = 6.6 Hz, 2H, $-OCH_2$) and 1.86–0.87 (m, 19H, 1 × CH_3, 8 × CH_2); MS (FAB+): m/z for $C_{24}H_{30}O_4$, calculated: 382.2, found: 382.7.

VIId. R_f = 0.27 (10% EtOAc–hexane); a colourless solid; yield: 0.68 g (87%); m.p = 75 °C; IR (KBr pellet): ν_{max} in cm^{-1} 2918, 2850, 1733, 1691, 1607, 1510, 1471 and 1257 cm^{-1}; ^{1}H NMR (400 MHz, $CDCl_3$): δ 10.02 (s, 1H, Ar-CHO), 8.14 (d, J = 8.4 Hz, 2H, Ar), 7.97 (d, J = 8.8 Hz, 2H, Ar), 7.41 (d, J = 8.4 Hz, 2H, Ar), 6.99 (d, J = 8.8 Hz, 2H, Ar), 4.06 (t, J = 6.4 Hz, 2H, $-OCH_2$) and 1.84–0.86 (m, 21H, 1 × CH_3, 9 × CH_2); MS (FAB+): m/z for $C_{25}H_{32}O_4$, calculated: 396.2, found: 396.5.

VIIe. R_f = 0.31 (10% EtOAc–hexane); a colourless solid; yield: 0.66 g (84%); m.p = 75.6 °C; IR (KBr pellet): ν_{max} in cm^{-1} 2918, 2851, 1737, 1698, 1603, 1580, 1510, 1471, 1422, 1397 and 1310 cm^{-1}, ^{1}H NMR (400 MHz, $CDCl_3$): δ 10.02 (s, 1H, Ar-CHO), 8.15 (d, J = 8.8 Hz, 2H, Ar), 7.97 (d, J = 8 Hz, 2H, Ar), 7.41 (d, J = 8.4 Hz, 2H, Ar), 6.99 (d, J = 8.8 Hz, 2H, Ar); 4.06 (t, J = 6.4 Hz, 2H, $-OCH_2$) and 1.86–0.86 (m, 23H, 1 × CH_3, 10 × CH_2); MS (FAB+): m/z for $C_{26}H_{34}O_4$, calculated: 410.3, found: 410.8.

4.2.6A. General procedure for the synthesis of (*S*)-4-{[(4-(octan-2-yloxy)phenyl)imino]methyl}phenyl 4-(*n*-alkoxy)benzoates. A mixture of 4-formylphenyl 4-(alkoxy)benzoate (**VIIa–e**) (0.4 mmol, 1 eq.) and (*S*)-4-(octan-2-yloxy)aniline (**IV**) (0.33 mmol, 1.2 eq.), catalytic amount of acetic acid in ethanol (10 mL) was refluxed under an inert atmosphere for 2 h. The colourless solid separated upon cooling the reaction mixture was collected by filtration, washed with ethanol and air-dried. The crude product was purified by repeated recrystallizations in absolute ethanol until the constant isotropization temperature was obtained.

SB(S)-8. A colourless solid; yield: 0.117 g (86%); $[\alpha]_D^{25}$ −5.8 (0.101%, CH_2Cl_2); IR (KBr pellet): ν_{max} in cm^{-1} 3451, 2924, 2852, 1739, 1608, 1577, 1510, 1467 and 1163; UV-vis: λ_{max} = 339.23 nm,

mol. conc. = 5.47 × 10^{-3} M, ε = 0.9874 × 10^2 L mol^{-1} cm^{-1}; ^{1}H NMR (400 MHz, $CDCl_3$): δ 8.49 (s, 1H, –CH═N), 8.16 (d, J = 8.8 Hz, 2H, Ar), 7.95 (d, J = 8.4 Hz, 2H, Ar), 7.32 (d, J = 8.4 Hz, 2H, Ar), 7.23 (d, J = 9.2 Hz, 2H, Ar), 6.99 (d, J = 9.2 Hz, 2H, Ar), 6.92 (d, J = 8.8 Hz, 2H, Ar), 4.38 (m, 1H, –O–CH–), 4.06 (t, J = 6.6 Hz, 2H, –OCH_2), 1.84–1.71 (m, 3H, –O–CH–CH_3) and 1.60–0.87 (m, 28H, 11 × CH_2, 2 × CH_3); ^{13}C NMR (100 MHz): 164.66, 163.72, 157.06, 157.04, 153.23, 144.60, 134.14, 132.37, 129.74, 122.23, 122.22, 121.32, 116.51, 114.40, 74.40, 68.40, 36.54, 31.83, 29.34, 29.32, 29.24, 29.12, 26.01, 25.55, 22.67, 22.63, 19.81, 14.11 and 14.09; anal. calcd for $C_{36}H_{47}NO_4$: C, 77.52; H, 8.49; N, 2.51. Found: C, 77.61; H, 8.56; N, 2.49.

***SB(S)*-9**. A colourless solid; yield: 0.120 g (82%); $[\alpha]_D^{25}$ −4.22 (0.099%, CH_2Cl_2); IR (KBr pellet): ν_{max} in cm^{-1} 3439, 2921, 2852, 1726, 1607, 1508, 1466 and 1166; UV-vis: λ_{max} = 340.47 nm, mol. conc. = 4.72 × 10^{-3} M, ε = 0.8257 × 10^2 L mol^{-1} cm^{-1}; ^{1}H NMR (400 MHz, $CDCl_3$): δ 8.48 (s, 1H, –CH═N), 8.15 (d, J = 8.8 Hz, 2H, Ar), 7.95 (d, J = 8.4 Hz, 2H, Ar), 7.32 (d, J = 8.4 Hz, 2H, Ar), 7.23 (d, J = 8.8 Hz, 2H, Ar), 6.98 (d, J = 9.2 Hz, 2H, Ar), 6.92 (d, J = 8.8 Hz, 2H Ar), 4.37 (m, 1H, –O–CH), 4.06 (t, J = 6.6 Hz, 2H, –OCH_2), 1.86–1.71 (m, 3H, –O–CH–CH_3) and 1.60–0.86 (m, 30H, 12 × CH_2, 2 × CH_3); ^{13}C NMR (100 MHz): 164.65, 163.72, 157.06, 157.03, 153.23, 144.61, 134.14, 132.37, 129.73, 122.22, 121.32, 116.51, 114.40, 74.39, 68.40, 36.54, 31.89, 31.83, 30.93, 29.53, 29.38, 29.31, 29.27, 29.12, 26.00, 25.55, 22.69, 22.62, 19.81, 14.11 and 14.09; anal. calcd for $C_{37}H_{49}NO_4$: C, 77.72; H, 8.64; N, 2.45. Found: C, 77.52; H, 8.66; N, 2.37.

***SB(S)*-10**. A colourless solid; yield: 0.128 g (82%); $[\alpha]_D^{25}$ −3.4 (0.102%, CH_2Cl_2); IR (KBr pellet): ν_{max} in cm^{-1} 3444, 2923, 2851, 1734, 1607, 1507, 1467 and 1167; UV-vis: λ_{max} = 339.41 nm, mol. conc. = 4.1 × 10^{-3} M, ε = 1.61 × 10^2 L mol^{-1} cm^{-1}; ^{1}H NMR (400 MHz, $CDCl_3$): δ 8.49 (s, 1H, –CH═N), 8.16 (d, J = 9.2 Hz, 2H, Ar), 7.95 (d, J = 8.4 Hz, 2H, Ar), 7.32 (d, J = 8.4 Hz, 2H, Ar), 7.23 (d, J = 8.8 Hz, 2H, Ar), 6.99 (d, J = 8.8 Hz, 2H, Ar), 6.92 (d, J = 8.8 Hz, 2H Ar), 4.39 (m, 1H, –O–CH), 4.06 (t, J = 6.6 Hz, 2H, –OCH_2), 1.86–1.71 (m, 3H, –O–CH–CH_3) and 1.60–0.87 (m, 32H, 13 × CH_2, 2 × CH_3); ^{13}C NMR (100 MHz): 164.65, 163.72, 157.06, 157.04, 153.23, 144.06, 134.14, 132.37, 129.74, 122.23, 122.22, 121.32, 116.51, 114.40, 74.40, 68.40, 36.54, 31.92, 31.83, 29.57, 29.38, 29.32, 29.12, 26.01, 25.55, 22.70, 22.63, 19.82, 14.12 and 14.09; Anal. calcd for $C_{38}H_{51}NO_4$: C, 77.91; H, 8.77; N, 2.39. Found: C, 77.71; H, 8.96; N, 2.55.

***SB(S)*-11**. A colourless solid; yield: 0.142 g (85%); $[\alpha]_D^{25}$ −5.4 (0.102%, CH_2Cl_2); IR (KBr pellet): ν_{max} in cm^{-1} 3451, 2925, 2856, 1736, 1608, 1508, 1467 and 1165; UV-vis: λ_{max} = 340.80 nm, mol. conc. = 3.92 × 10^{-3} M, ε = 1.0464 × 10^2 L mol^{-1} cm^{-1}; ^{1}H NMR (400 MHz, $CDCl_3$): δ 8.49 (s, 1H, –CH═N), 8.16 (d, J = 8.8 Hz, 2H, Ar), 7.96 (d, J = 8.8 Hz, 2H, Ar), 7.32 (d, J = 8.8 Hz, 2H, Ar), 7.23 (d, J = 8.8 Hz, 2H, Ar), 6.99 (d, J = 8.8 Hz, 2H, Ar), 6.92 (d, J = 8.8 Hz, 2H Ar), 4.38 (m, 1H, –O–CH), 4.06 (t, J = 6.6 Hz, 2H, –OCH_2), 1.86–1.71 (m, 3H, –O–CH–CH_3) and 1.62–0.87 (m, 34H, 14 × CH_2, 2 × CH_3); ^{13}C NMR (100 MHz): 164.65, 163.72, 157.06, 157.04, 153.23, 144.60, 134.14, 132.37, 129.74, 122.23, 122.22, 121.32, 116.51, 114.40, 74.39, 68.40, 36.54, 31.93, 31.83, 29.63, 29.61, 29.58, 29.38, 29.36, 29.32, 29.12, 26.00, 25.56, 22.71, 22.63, 19.82, 14.13 and 14.09; anal. calcd for $C_{39}H_{53}NO_4$: C, 78.09; H, 8.91; N, 2.34. Found: C, 78.24; H, 9.01; N, 2.24.

***SB(S)*-12**. A colourless solid; yield: 0.152 g (84%); $[\alpha]_D^{25}$ −6.70 (0.101%, CH_2Cl_2); IR (KBr pellet): ν_{max} in cm^{-1} 3451, 2925, 2857, 1736, 1608, 1508, 1466 and 1165; UV-vis: λ_{max} = 340.94 nm, mol. conc. = 5.1 × 10^{-3} M, ε = 1.0098 × 10^2 L mol^{-1} cm^{-1}, ^{1}H NMR (400 MHz, $CDCl_3$): δ 8.49 (s, 1H, –CH═N), 8.16 (d, J = 8.8 Hz, 2H, Ar), 7.96 (d, J = 8.8 Hz, 2H, Ar), 7.32 (d, J = 8.4 Hz, 2H, Ar), 7.23 (d, J = 8.8 Hz, 2H, Ar), 6.99 (d, J = 9.2 Hz, 2H, Ar), 6.92 (d, J = 8.8 Hz, 2H Ar), 4.39 (m, 1H, –O–CH), 4.06 (t, J = 6.6 Hz, 2H, –OCH_2), 1.86–1.71 (m, 3H, –O–CH–CH_3) and 1.57–0.87 (m, 36H, 15 × CH_2, 2 × CH_3); ^{13}C NMR (100 MHz): 164.64, 163.72, 157.07, 157.02, 153.23, 144.61, 134.14, 132.37, 129.73, 122.23, 122.21, 121.32, 116.51, 114.40, 74.39, 68.40, 36.54, 31.94, 31.83, 30.93, 29.68, 29.66, 29.61, 29.58, 29.37, 29.32, 29.12, 26.01, 25.56, 22.71, 22.63, 19.82, 14.13 and 14.09; anal. calcd for $C_{40}H_{55}NO_4$: C, 78.26; H, 9.03; N, 2.28. Found: C, 78.34; H, 9.30; N, 2.05.

4.2.6B. General procedure for the synthesis of (*R*)-4-{[(4-(octan-2-yloxy)phenyl)imino]methyl}phenyl 4-(*n*-alkoxy)benzoates. A mixture of 4-formylphenyl 4-(*n*-alkoxy)benzoate (**VIIa–e**) (0.4 mmol, 1 eq.) and (*R*)-4-(octan-2-yloxy)aniline (**II**) (0.33 mmol, 1.2 eq.), catalytic amount of acetic acid in ethanol (10 mL) was refluxed under an inert atmosphere for 2 h. The white solid separated upon cooling the reaction mixture was collected by filtration, washed with ethanol and air-dried. The crude product was purified by repeated recrystallizations from absolute ethanol until the constant isotropization temperature was noted.

***SB(R)*-8**. A colourless solid; yield: 0.122 g (83%); $[\alpha]_D^{25}$ +6.01 (0.098%, CH_2Cl_2); IR (KBr pellet): ν_{max} in cm^{-1} 3446, 2925, 2856, 1737, 1607, 1507,1467 and 1165; UV-vis: λ_{max} = 340.99 nm, mol. conc. = 6.99 × 10^{-3} M, ε = 0.4147 × 10^2 L mol^{-1} cm^{-1}; ^{1}H NMR (400 MHz, $CDCl_3$): δ 8.49 (s, 1H, –CH═N), 8.16 (d, J = 8.4 Hz, 2H, Ar), 7.95 (d, J = 8 Hz, 2H, Ar), 7.32 (d, J = 8.4 Hz, 2H, Ar), 7.23 (d, J = 8.4 Hz, 2H, Ar), 6.98 (d, J = 8.4 Hz, 2H, Ar), 6.92 (d, J = 8.4 Hz, 2H Ar), 4.38 (m, 1H, –O–CH), 4.06 (t, J = 6.4 Hz, 2H, –OCH_2), 1.86–1.72 (m, 3H, –O–CH–CH_3) and 1.60–0.89 (m, 28H, 11 × CH_2, 2 × CH_3); ^{13}C NMR (100 MHz): 164.59, 163.68, 156.96, 153.19, 144.57, 134.1, 132.32, 129.69, 122.18, 121.29, 116.47, 114.35, 74.35, 68.36, 36.50, 31.78, 29.30, 29.27, 29.08, 25.97, 25.51, 22.63, 22.58, 19.77 and 14.05; anal. calcd for $C_{36}H_{47}NO_4$: C, 77.52; H, 8.49; N, 2.51. Found: C, 77.30; H, 8.49; N, 2.42.

***SB(R)*-9**. A colourless solid; yield: 0.135 g (82%); $[\alpha]_D^{25}$ +4.22 (0.099%, CH_2Cl_2); IR (KBr pellet): ν_{max} in cm^{-1} 3441, 2922, 2854, 1726, 1608, 1506,1465 and 1166; UV-vis: λ_{max} = 340.79 nm, mol. conc. = 7.87 × 10^{-3} M, ε = 1.2198 × 10^2 L mol^{-1} cm^{-1}; ^{1}H NMR (400 MHz, $CDCl_3$): δ 8.49 (s, 1H, –CH═N), 8.16 (d, J = 8.4 Hz, 2H, Ar), 7.96 (d, J = 8.4 Hz, 2H, Ar), 7.32 (d, J = 8.4 Hz, 2H, Ar), 7.23 (d, J = 8.4 Hz, 2H, Ar), 6.99 (d, J = 8.8 Hz, 2H, Ar), 6.92 (d, J = 8.4 Hz, 2H, Ar), 4.38 (m, 1H, –O–CH), 4.06 (t, J = 6.4 Hz, 2H, –OCH_2), 1.84–1.72 (m, 3H, –O–CH–CH_3) and 1.59–0.89 (m, 30H, 12 × CH_2, 2 × CH_3); ^{13}C NMR (100 MHz): 164.6, 163.68, 156.98, 153.19, 144.57, 134.10, 132.33, 129.69, 122.18, 121.28, 116.47, 114.36, 74.35, 68.36, 36.50, 31.79, 29.35,29.28, 29.23, 29.09, 25.97, 25.52, 22.65, 22.59, 19.78 and

14.06; anal. calcd for $C_{37}H_{49}NO_4$: C, 77.72; H, 8.64; N, 2.45. Found: C, 77.65; H, 8.62; N, 2.72.

***SB(R)*-10**. A colourless solid; yield: 0.158 g (84%); $[\alpha]_D^{25}$ +3.02 (0.099%, CH_2Cl_2); IR (KBr pellet): ν_{max} in cm^{-1} 3445, 2924, 2853, 1734, 1607, 1506,1467 and 1166; UV-vis: λ_{max} = 341.01 nm, mol. conc. = 3.76×10^{-3} M, $\varepsilon = 1.1449 \times 10^2$ L mol^{-1} cm^{-1}; ^{1}H NMR (400 MHz, $CDCl_3$): δ 8.49 (s, 1H, –CH═N), 8.16 (d, J = 8.8 Hz, 2H, Ar), 7.95 (d, J = 8.4 Hz, 2H, Ar), 7.32 (d, J = 8.4 Hz, 2H, Ar), 7.23 (d, J = 8.8 Hz, 2H, Ar), 6.99 (d, J = 8.8 Hz, 2H, Ar), 6.92 (d, J = 8.8 Hz, 2H, Ar), 4.38 (m, 1H, –O–CH), 4.07 (t, J = 6.4 Hz, 2H, $-OCH_2$), 1.86–1.71 (m, 3H, $-O-CH-CH_3$) and 1.49–0.87 (m, 32H, 13 × CH_2, 2 × CH_3); ^{13}C NMR (100 MHz): 164.60, 163.67, 156.97, 153.19, 144.57, 134.10, 132.32, 129.69, 122.17, 121.28, 116.47, 114.35, 74.35, 68.35, 36.50, 31.87, 31.78, 29.52, 29.33, 29.27, 29.07, 25.96, 25.50, 22.65, 22.58, 19.77 and 14.07; anal. calcd for $C_{38}H_{51}NO_4$: C, 77.91; H, 8.77; N,2.39. Found: C, 77.51; H, 8.88; N, 2.56.

***SB(R)*-11**. A colourless solid; yield: 0.138 g (86%); $[\alpha]_D^{25}$ +6.63 (0.10%, CH_2Cl_2); IR (KBr pellet): ν_{max} in cm^{-1} 3439, 2920, 2851, 1729, 1606, 1507 and 1166; UV-vis: λ_{max} = 340.57 nm, mol. conc. = 8.17×10^{-3} M, $\varepsilon = 1.5056 \times 10^2$ L mol^{-1} cm^{-1}; ^{1}H NMR (400 MHz, $CDCl_3$): δ 8.54 (s, 1H, –CH═N), 8.21 (d, J = 8.8 Hz, 2H, Ar), 8.01 (d, J = 8.8 Hz, 2H, Ar), 7.37 (d, J = 8.4 Hz, 2H, Ar), 7.28 (d, J = 8.8 Hz, 2H, Ar), 7.04 (d, J = 9.2 Hz, 2H, Ar), 6.98 (d, J = 8.8 Hz, 2H, Ar), 4.38 (m, 1H, –O–CH), 4.06 (t, J = 6.6 Hz, 2H, $-OCH_2$), 1.86–1.71 (m, 3H, $-O-CH-CH_3$) and 1.62–0.87 (m, 34H, 14 × CH_2, 2 × CH_3); ^{13}C NMR (100 MHz): 164.61, 163.69, 156.98, 153.21, 144.58, 134.12, 132.34, 129.70, 122.19, 121.30, 116.48, 114.36, 74.36, 68.36, 36.51, 31.90, 31.80, 31.58, 29.58, 29.33, 29.09, 25.98, 25.53, 22.60, 19.78 and 14.09; anal. calcd for $C_{39}H_{53}NO_4$: C, 78.09; H, 8.91; N, 2.34. Found: C, 77.98; H, 8.93; N, 2.55.

***SB(R)*-12**. A colourless solid; yield: 0.142 g (85%); $[\alpha]_D^{25}$ +7.24 (0.104%, CH_2Cl_2); IR (KBr pellet): ν_{max} in cm^{-1} 3439, 2920, 2849, 1726, 1607, 1506,1467 and 1164; UV-vis: λ_{max} = 340.85 nm, mol. conc. = 5.38×10^{-3} M, $\varepsilon = 2.232 \times 10^2$ L mol^{-1} cm^{-1}; ^{1}H NMR (400 MHz, $CDCl_3$): δ 8.48 (s, 1H, –CH═N), 8.15 (d, J = 8.8 Hz, 2H, Ar), 7.95 (d, J = 8.4 Hz, 2H, Ar), 7.32 (d, J = 8.8 Hz, 2H, Ar), 7.23 (d, J = 8.8 Hz, 2H, Ar), 6.98 (d, J = 8.8 Hz, 2H, Ar), 6.92 (d, J = 8.8 Hz, 2H, Ar), 4.38 (m, 1H, –O–CH), 4.06 (t, J = 6.6 Hz, 2H, $-OCH_2$), 1.84–1.71 (m, 3H, $-O-CH-CH_3$) and 1.60–0.87 (m, 36H, 15 × CH_2, 2 × CH_3); ^{13}C NMR (100 MHz): 164.63, 163.71, 157.05, 157.01, 153.22, 144.59, 134.13, 132.35, 129.72, 122.22, 122.20, 121.31, 116.50, 114.38, 74.38, 68.39, 36.53, 31.93, 31.82, 30.91, 29.66, 29.64, 29.59, 29.56, 29.36, 29.11, 25.99, 25.54, 22.70, 22.61, 19.80, 14.12 and 14.08; anal. calcd for $C_{40}H_{55}NO_4$: C, 78.26; H, 9.03; N, 2.28. Found: C, 78.22; H, 9.05; N, 2.14.

Acknowledgements

CVY expresses his deep sense of gratitude to the Department of Science and Technology (DST), New Delhi, Govt. of India, for the financial support through SERB project No. SR/S1//OC-04/2012.

References

1 (*a*) P. G. De Gennes and J. Prost, *The Physics of Liquid Crystals*, Oxford Science Publication, Oxford, 1993; (*b*) S. Chandrasekhar, *Liquid Crystals.*, Cambridge University Press, 2nd edn, 1994; (*c*) P. J. Collings and M. Hird, *Introduction to Liquid Crystals Chemistry and Physics*, Taylor and Francis Ltd., London, 1997; (*d*) B. Bahadur, *Liquid Crystals: Application and Uses*, World Scientific, Singapore, 1990, vol. 1–3; (*e*) *Handbook of Liquid Crystals: Fundamentals*, ed. J. W. Goodby, P. J. Collings, T. Kato, C. Tschierske, H. Gleeson and P. Raynes, Wiley-VCH, Weinheim, Germany, 2014, vol. 1; (*f*) T. Geelhaar, K. Griesar and B. Reckmann, *Angew. Chem., Int. Ed.*, 2013, **52**, 8798.

2 (*a*) M. Bremer, P. Kirsch, M. Klasen-Memmer and K. Tarumi, *Angew. Chem., Int. Ed.*, 2013, **52**, 8880; (*b*) *Competing for the future How Digital Innovations are Changing the World; – Principles of LCD displays*, ed. H. Kressel and T. V. Lento, Cambridge University Press, 2007, Appendix 1.9, pp. 374–376; (*c*) R. H. Chen, *Liquid Crystal Displays: Fundamental Physics and Technology*, Wiley-SID Series in Display Technology, Wiley, 2011; (*d*) D.-K. Yang and S. T. Wu, *Fundamentals of Liquid Crystal Devices*, Wiley-SID Series in Display Technology, Wiley, 2nd edn, 2014.

3 (*a*) *Materials Chirality: Volume 24 of Topics in Stereochemistry*, ed. M. M. Green, R. J. M. Nolte and E. W. Meijer, John Wiley & Sons Inc., New Jersey, 2003; (*b*) *Chirality in Liquid Crystals*, ed. H.-S. Kitzerow and C. Bahr, Springer-Verlag, New York, 2001; (*c*) For a very recent review on chiral liquid crystals see: I. Dierking, *Symmetry*, 2014, **6**, 444(*d*) *Nanoscience with Liquid Crystals: From Self-Organized Nanostructures to Applications*, ed. Q. Li, Springer, 2014; (*e*) *Liquid Crystals Beyond Displays: Chemistry, Physics, and Applications*, John Wiley & Sons, 2012; (*f*) H. K. Bisoyi and Q. Li, *Acc. Chem. Res.*, 2014, **47**, 3184; (*g*) T.-H. Lin, Y. Li, C.-T. Wang, H.-C. Jau, C.-W. Chen, C.-C. Li, H. K. Bisoyi, T. J. Bunning and Q. Li, *Adv. Mater.*, 2013, **25**, 5050; (*h*) Y. Wang and Q. Li, *Adv. Mater.*, 2012, **24**, 1926.

4 (*a*) For an excellent research review on chemistry of FLCs see: M. Hird, *Liq. Cryst.*, 2011, **38**, 1467 and references cited therein; (*b*) S. T. Lagerwall, *Ferroelectrics*, 2004, **301**, 15; (*c*) J. W. Goodby, R. Blinc, N. A. Clark, S. T. Lagerwall, M. A. Osipov, S. A. Pikin, T. Sakurai, K. Yoshino and B. Zenks, *Ferroelectric Liquid Crystals. Principle and Applications*, Gordon and Breach, Philadelphia, 1991; (*d*) S. T. Lagerwall, *Ferroelectric and Antiferroelectric Liquid Crystals*, Wiley-VCH, Weinheim, 1999; (*e*) S. J. J. Elston, *J. Mod. Opt.*, 1995, **42**, 19; (*f*) J. W. Goodby, *J. Mater. Chem.*, 1991, **1**, 307; (*g*) H. Takezoe, *Ferroelectric, Antiferroelectric and Ferroelectric Liquid Crystals: Applications, Encyclopedia of Materials: Science and Technology*, Elsevier Science Ltd, 2001; (*h*) S. T. Lagerwall, Ferroelectric liquid crystals, in *Low molecular weight liquid crystals II*, ed. D. Demus, J. Goodby, G. W. Gray, H.-W. Spiess and V. Vill, Wiley-VCH, Weinheim, 1998, vol. 2B, pp. 515–664; (*i*) I. Musevic, R. Blinc and B. Zeks, *The Physics of Ferroelectric and Antiferroelectric Liquid Crystals*, World Scientific, Singapore, 2000.

5 (*a*) D. M. Walba, *Science*, 1995, **270**, 250; (*b*) J. Prakash, D. S. Mehta and A. M. Biradar, *Deformed helix ferroelectric liquid crystals: Materials for displays*, Lambert Academy Publishing, 2013.
6 P. A. Kumar and V. G. K. M. Pisipati, *Adv. Mater.*, 2000, **12**, 1617.
7 (*a*) F. Guittard, E. T. de Givenchy, S. Geribaldi and A. Cambon, *J. Fluorine Chem.*, 1999, **100**, 85; (*b*) K. M. Fergusson and M. Hird, *J. Mater. Chem.*, 2010, **20**, 3069; (*c*) D. M. Walba, in *Advances in the Synthesis and Reactivity of Solids*, ed. T. E. Mallouck, JAI Press, Ltd, Greenwich, CT, 1991; (*d*) M. Hird, *Chem. Soc. Rev.*, 2007, **36**, 2070; (*e*) S. M. Kelly, *Helv. Chim. Acta*, 1989, **72**, 595; (*f*) V. Vill, *LiqCryst database*, www.lcipublisher.com/liqcryst.html.
8 (*a*) J. W. Goodby, E. Chin and J. S. Patel, *J. Phys. Chem.*, 1989, **93**, 8067; (*b*) W. Kuczynski and H. Stegemeyer, *Chem. Phys. Lett.*, 1980, **70**, 123; (*c*) H. Stegemeyer, R. Meister, H. Hoffmann, A. Sprick and A. Becker, *J. Mater. Chem.*, 1995, **5**, 2183; (*d*) M. A. Osipov, H. Stegemeyer and A. Sprick, *Phys. Rev. E: Stat. Phys., Plasmas, Fluids, Relat. Interdiscip. Top.*, 1996, **54**, 6387; (*e*) E. V. Popova, T. G. Drushlyak, V. V. Vashchenko, A. P. Fedoryako and L. A. Kutulya, *J. Phys. Chem.*, 2002, **76**, 1779.
9 (*a*) M. J. Bradshaw, V. Brimmell and E. P. Raynes, *Liq. Cryst.*, 1987, **2**, 107; (*b*) V. Brimmell, J. Constant, H. A. Pedlingham, E. P. Raynes and A. K. Samra, *Liq. Cryst.*, 1989, **6**, 545; (*c*) M. Chambers, R. Clemitson, D. Coates, S. Greenfield, J. A. Jenner and I. C. Sage, *Liq. Cryst.*, 1989, **5**, 153; (*d*) L. K. M. Chan, G. W. Gray and D. Lacey, *Mol. Cryst. Liq. Cryst.*, 1985, **123**, 185; (*e*) G. W. Gray, M. Hird, D. Lacey and K. J. Toyne, *J. Chem. Soc., Perkin Trans. 2*, 1989, 2041; (*f*) M. E. Glendenning, J. W. Goodby, M. Hird and K. J. Toyne, *J. Chem. Soc., Perkin Trans. 2*, 2000, 27; (*g*) J. W. Goodby, *Angew. Chem., Int. Ed. Engl.*, 2008, **47**, 2754.
10 (*a*) D. S. Shankar Rao, S. Krishna Prasad, V. N. Raja, C. V. Yelamaggad and S. A. Nagamani, *Phys. Rev. Lett.*, 2001, **87**, 085504; (*b*) C. V. Yelamaggad, U. S. Hiremath, D. S. Shankar Rao and S. Krishna Prasad, *Chem. Commun.*, 2000, 57; (*c*) C. V. Yelamaggad, G. Shanker, U. S. Hiremath and S. K. Prasad, *J. Mater. Chem.*, 2008, **18**, 2927 and the references cited therein; ; (*d*) U. S. Hiremath, G. M. Sonar, D. S. Shankar Rao and C. V. Yelamaggad, *J. Mater. Chem.*, 2011, **21**, 4064; (*e*) C. V. Yelamaggad, I. Shashikala, G. Liao, D. S. Shankar Rao, S. Krishna Prasad, Q. Li and A. Jakli, *Chem. Mater.*, 2006, **18**, 6100; C. V. Yelamaggad, A. S. Achalkumar, N. L. Bonde and A. K. Prajapati, *Chem. Mater.*, 2006, **18**, 1076; (*f*) J.-W. Lee, D. K. Oh, C. V. Yelamaggad, S. Anitha Nagamani and J.-I. Jin, *J. Mater. Chem.*, 2002, **12**, 2225; (*g*) C. V. Yelamaggad, A. S. Achalkumar, D. S. Shankar Rao and S. Krishna Prasad, *Org. Lett.*, 2007, **9**, 2641.
11 G. Shanker and C. V. Yelamaggad, *J. Mater. Chem.*, 2011, **21**, 15279.
12 G. Shanker and C. V. Yelamaggad, *J. Phys. Chem. B*, 2011, **115**, 10849.
13 C. V. Yelamaggad and G. Shanker, *Tetrahedron*, 2008, **64**, 3760.
14 G. Shanker and C. V. Yelamaggad, *New J. Chem.*, 2012, **36**, 918.
15 C. V. Yelamaggad and G. Shanker, *Liq. Cryst.*, 2007, **34**, 799.
16 A. S. Achalkumar, D. S. S. Rao and C. V. Yelamaggad, *New J. Chem.*, 2014, **38**, 4235.
17 (*a*) J. W. Goodby and T. M. Leslie, *Mol. Cryst. Liq. Cryst.*, 1984, **110**, 175; (*b*) J. W. Goodby, *Liquid Crystals and Ordered Fluids*, ed. J. Johnson and A. C. Griffin, Plenum, New York, 1984, vol. 4, pp. 175–201; (*c*) J. W. Goodby, Properties and structures of ferroelectric liquid crystals, in *Ferroelectric liquid crystals*, ed. G. W. Taylor, Gordon and Breach, Philadelphia, 1991, vol. 7, pp. 99–248.
18 (*a*) W. Helfrich and C. S. Oh, *Mol. Cryst. Liq. Cryst.*, 1971, **14**, 289; (*b*) I. A. Radini and M. Hird, *Liq. Cryst.*, 2009, **36**, 1417; (*c*) M. F. Bone, M. J. Bradshaw, L. K. M. Chan, D. Coates, J. Constant, P. A. Gemmell, G. W. Gray, D. Lacey and K. J. Toyne, *Mol. Cryst. Liq. Cryst.*, 1988, **164**, 117; (*d*) K. Yoshino, M. Ozaki, H. Taniguchi, M. Ito, K. Satoh, N. Yamasaki and T. Kitazume, *Jpn. J. Appl. Phys.*, 1987, **26**, L77; (*e*) T. Hirai, M. Fukumasa, I. Nishiyama, A. Yoshizawa, N. Shiratori, A. Yokoyama and M. Yamane, *Ferroelectrics*, 1991, **114**, 251; (*f*) A. D. L. Chandani, Y. Ouchi, H. Takezoe and A. Fukuda, *Jpn. J. Appl. Phys.*, 1989, **28**, L1261–L1264; (*g*) A. Fukuda, Y. Takanishi, T. Isozaki, K. Ishikawa and H. Takezoe, *J. Mater. Chem.*, 1994, **4**, 997; (*h*) A. Yoshizawa, I. Nishiyama, M. Fukumassa, T. Hirai and M. Yamne, *Jpn. J. Appl. Phys.*, 1989, **28**, L1269–L1271; (*i*) N. Shiratori, A. Yoshizawa, I. Nishiyama, M. Fukumasa, A. Yokoyama, T. Hirai and M. Yamane, *Mol. Cryst. Liq. Cryst.*, 1991, **199**, 129; (*j*) J. S. Dave, M. R. Menon and P. R. Pate, *Mol. Cryst. Liq. Cryst.*, 2001, **364**, 575; (*k*) M. Stojanovic, A. Bubnov, D. Z. Obadovic, V. Hamplova, M. Kaspar and M. Cvetinov, *Phase Transitions*, 2011, **84**, 380; (*l*) S. J. Cowling, A. W. Hall and J. W. Goodby, *Liq. Cryst.*, 2005, **32**, 1483; (*m*) A. A. Merlo, H. Gallardo and T. R. Taylor, *Quim. Nova*, 2001, **24**, 354; (*n*) A. Merlo, H. Gallardo, T. R. Taylor and T. Kroin, *Mol. Cryst. Liq. Cryst.*, 1994, **250**, 31.
19 (*a*) O. Mitsunobu and Y. Yamada, *Bull. Chem. Soc. Jpn.*, 1967, **40**, 2380; (*b*) O. Mitsunobu, *Synthesis*, 1981, 1.
20 (*a*) D. Pucci, O. Franescangeli and M. Ghedini, *Mol. Cryst. Liq. Cryst.*, 2001, **372**, 51; (*b*) J. del Barrio, R. M. Tejedor, L. S. Chinelatto, C. Sanchez, M. Pinol and L. Oriol, *J. Mater. Chem.*, 2009, **19**, 4922–4930.
21 N. Kirov and H. Ratajczak, *J. Mol. Struct.*, 1980, **61**, 207.
22 A. Hassnei and V. Alexanian, *Tetrahedron Lett.*, 1978, 4475.
23 K. Muhammad, S. Hameed, J. Tan and R. Liub, *Liq. Cryst.*, 2011, **38**, 333.
24 I. Dierking, *Textures of Liquid Crystals*, Wiley-VCH Verlag GmbH & Co. KGaA, 2003.
25 (*a*) M. D. Radcliffe, M. L. Brostrom, K. A. Epstein, A. G. Rappaport, B. N. Thomas, R. Shao and N. A. Clark, *Liq. Cryst.*, 1999, **26**, 789; (*b*) J. C. Roberts, N. Kapernaum, Q. Song, D. Nonnenmacher, K. Ayub, F. Giesselmann and R. P. Lemieux, *J. Am. Chem. Soc.*, 2010, **132**, 364; (*c*) U. S. Hiremath, H. M. Menezes, G. G. Nair, D. S. Shankar Rao and S. K. Prasad, *J. Mater. Chem. C*, 2013, **1**, 5799.
26 M. K. Reddy, K. S. Reddy, K. Yoga, M. Prakash, T. Narasimhaswamy, A. B. Mandal, N. P. Lobo, K. V. Ramanathan,

D. S. Shankar Rao and S. Krishna Prasad, *J. Phys. Chem. B*, 2013, **117**, 5718.

27 (*a*) F. D. Saeva, in *Liquid Crystals, the Fourth State of Matter*, ed. F. D. Saeva, Marcel Dekker, New York, 1979, p. 249; (*b*) G. Solladie and R. G. Zimmermann, *Angew. Chem., Int. Ed.*, 1984, **23**, 348; (*c*) F. D. Saeva, *J. Am. Chem. Soc.*, 1972, **94**, 5135; (*d*) X. M. Dong and D. G. Gray, *Langmuir*, 1997, **13**, 3029; (*e*) M. M. Green, S. Zanella, H. Gu, T. Sato, G. Gottarelli, S. K. Jha, G. P. Spada, A. M. Schoevaars, B. Feringa and A. Teramoto, *J. Am. Chem. Soc.*, 1998, **120**, 9810; (*f*) B. R. Harkness and D. G. Gray, *Macromolecules*, 1991, **24**, 1800; (*g*) J. Yoshida, H. Sato, A. Yamagishi and N. Hoshino, *J. Am. Chem. Soc.*, 2005, **127**, 8453; (*h*) N. Hoshino, Y. Matsuoka, K. Okamoto and A. Yamagishi, *J. Am. Chem. Soc.*, 2003, **125**, 1718; (*i*) T. Mitsuoka, H. Sato, J. Yoshida, A. Yamagishi and Y. Einaga, *Chem. Mater.*, 2006, **18**, 3442; (*j*) H. Qi, J. O. Neil and T. Hegmann, *J. Mater. Chem.*, 2008, **18**, 374.

28 (*a*) K. Yamada, Y. Takanishi, K. Ishikawa, H. Takezoe, A. Fukuda and M. A. Osipov, *Phys. Rev. E: Stat. Phys., Plasmas, Fluids, Relat. Interdiscip. Top.*, 1997, **56**, R43(R); (*b*) Y. Takanishi, T. Ogasawara, A. Yoshizawa, J. Umezawa, T. Kusumoto, T. Hiyama, K. Ishikawaa and H. Takezoea, *J. Mater. Chem.*, 2002, **12**, 1325; (*c*) C. J. Boulton, J. G. Finden, E. Yuh, J. J. Sutherland, M. D. Wand, G. Wu and R. P. Lemieux, *J. Am. Chem. Soc.*, 2005, **127**, 13656.

29 (*a*) *Circular Dichroism: Principles and Applications*, ed. N. Berova, K. Nakanishi and R. W. Woody, Wiley-VCH, New York, 2nd edn, 2000; (*b*) *Circular Dichroism: Theory and Spectroscopy*, ed. D. S. Rodgers, Nova Publishers, New York, USA, 2011.